SOLUTION PROCESSABLE BENZOTRIAZOLE, BENZIMIDAZOLE AND BIPHENYL CONTAINING CONJUGATED COPOLYMERS FOR OPTOELECTRONIC APPLICATIONS

A THESIS SUBMITTED TO
THE GRADUATE SCHOOL OF NATURAL AND APPLIED SCIENCES
OF
MIDDLE EAST TECHNICAL UNIVERSITY

BY

TUĞBA KAYA DENİZ

IN PARTIAL FULFILLMENT OF THE REQUIREMENTS
FOR
THE DEGREE OF MASTER OF SCIENCE
IN
POLYMER SCIENCE AND TECHNOLOGY

SEPTEMBER 2012

Approval of the thesis:

SOLUTION PROCESSABLE BENZOTRIAZOLE, BENZIMIDAZOLE AND BIPHENYL CONTAINING CONJUGATED COPOLYMERS FOR OPTOELECTRONIC APPLICATIONS

Submitted by **TUĞBA KAYA DENİZ** in partial fulfillment of the requirements for the degree of **Master of Science in Polymer Science and Technology Department, Middle East Technical University** by,

Prof. Dr. Canan Özgen _____
Dean, Graduate School of **Natural and Applied Sciences**

Prof. Dr. Necati Özkan _____
Head of Department, **Polymer Science and Technology**

Assoc. Prof. Dr. Ali Çırpan _____
Supervisor, **Chemistry Department**

Examining Committee Members:

Prof. Dr. Teoman Tinçer
Chemistry Dept., METU _____

Assoc. Prof. Dr. Ali Çırpan
Chemistry Dept., METU _____

Prof. Dr. Levent Toppare
Chemistry Dept., METU _____

Assist. Prof. Dr. Emren Nalbant Esentürk
Chemistry Dept., METU _____

Assoc. Dr. Yasemin Arslan Udum
Chemistry Dept., Gazi University _____

Date: _____

I hereby declare that all information in this document has been obtained and presented in accordance with academic rules and ethical conduct. I also declare that, as required by these rules and conduct, I have fully cited and referenced all material and results that are not original to this work.

Name, Last Name: TUĞBA KAYA DENİZ

Signature :

ABSTRACT

SOLUTION PROCESSABLE BENZOTRIAZOLE, BENZIMIDAZOLE AND BIPHENYL CONTAINING CONJUGATED COPOLYMERS FOR OPTOELECTRONIC APPLICATIONS

Deniz, Tuğba Kaya
M.S., Department of Polymer Science and Technology
Supervisor : Assoc. Prof. Dr. Ali Çırpan

September 2012, 73 pages

The synthesis and optoelectronic properties of biphenyl based conjugated copolymers with varying acceptor units in the polymer backbone were investigated. The well known Donor-Acceptor Theory was used to establish the synthetic pathway for the structural modifications. Solubility issues regarding biphenyl polymer was solved by copolymerizing with soluble units. For this purpose; poly 4-(biphenyl-4-yl)-4'-tert butylspiro[benzo[d]imidazole-2,1'-cyclohexane] (P1), poly 4-(biphenyl-4-yl)-2- dodecyl-2H-benzo[d][1,2,3]triazole (P2) and poly(4-(5-(biphenyl-4-yl)-4-hexyl-thiophen-2-yl)-2-dodecyl-7-(4-hexylthiophen-2-yl)-2H-benzo[d][1,2,3]triazole (P3) were synthetized using Suzuki coupling process. Electrochemical properties of these polymers were examined by cyclic voltammetry, spectroelectrochemistry and kinetic studies. Polymers P2 and P3 showed both p- and n-doping behaviors and multi-colored electrochromic states. Optical studies revealed that emission color of biphenyl is tuned from blue to orange and the polymers are good candidates for light emitting diode applications. OLED application of P3 was established and outputs of the device were increased by energy transfer studies. The preliminary investigation indicated

that P3 possesses promising efficiencies.

Keywords: Benzotriazole, Biphenyl, Optoelectronic, Organic Light-Emitting Diodes, Conjugated Copolymer

ÖZ

OPTOELEKTRONİK UYGULAMALAR İÇİN ÇÖZÜNEBİLEN BENZOTRİAZOL, BENZİMİDAZOL VE BİFENİL İÇEREN KONJUGE KOPOLİMERLER

Deniz, Tuğba Kaya
Yüksek Lisans, Polimer Bilimi ve Teknolojileri Bölümü
Tez Yöneticisi : Doç. Dr. Ali Çırpan

Eylül 2012, 73 sayfa

Polimer zinciri üzerinde değişik akseptör üniteleri kullanılarak sentezlenmiş bifenil bazlı konjüge polimerlerin optoelektronik özellikleri incelenmiştir. Sıklıkla kullanıla gelen Donör-Akseptör Teorisi yardımı ile yapısal değişikliklerle ilgili sentez yolu oluşturulmuştur. Bifenil bazlı polimerlerin sahip olduğu çözünürlük sorunu çözünür üniteler ile kopolimerizasyon işlemi gerçekleştirilerek giderilmiştir. Bu amaçla poly 4-(biphenyl-4-yl)-4'-tert butylspiro[benzo[d]imidazole-2,1'-cyclohexane] (P1), poly 4-(biphenyl-4-yl)-2- dodecyl-2H-benzo[d][1,2,3]triazole (P2) ve poly(4-(5-(biphenyl-4-yl)-4-hexylthiophen-2-yl)-2-dodecyl-7-(4-hexylthiophen-2-yl)-2H-benzo[d][1,2,3]-triazole (P3) polimerleri Suzuki birleşme yöntemi kullanılarak sentezlenmiştir. Bu polimerlerin elektrokimyasal özellikleri dönüşümlü voltametre, spektroelektrokimya ve kinetik çalışmalarla incelenmiştir . P2 ve P3 polimerlerinin p- ve n-tipi katkılanabilme ve multikromizm özelliklerine sahip oldukları gözlenmiştir. Optik çalışmalar bifenil için mavi olan emisyon renginin turuncuya kadar kaydırıldığını ve bu polimerlerin ışık yayan diyot uygulamaları için uygun adaylar olduklarını göstermiştir. P3 polimerinin OLED uygulaması gerçekleştirilmiş ve enerji transfer çalışmaları yardımı

ile cihaz verimliliği artırılmış ve elde edilen verimlilik seviyelerinin umut verici olduğu değerlendirilmiştir.

Anahtar Kelimeler: Benzotriazol, Bifenil, Optoelektronik, Organik Işık Yayan Diyotlar, Konjüge Kopolimer

To My Brother..

ACKNOWLEDGMENTS

I would like to express my sincere gratitude to the excellent and diligent guidance of Assoc. Prof. Dr. Ali Çırpan for his valuable suggestion, stimulating advice, creative and energetic instructions. I would also like to express my gratitude to Prof. Dr. Levent Toppare for his invaluable guidance. Moreover I am greatfull for the technical support by Assist. Prof. Dr. H. Emrah Ünalan.

I would like to thank to Ayda G. Nurioğlu, Doğukan Hazar Apaydın for their experimental helps beside their friendships.

I would like to thank to Melike Karakus, Seval Ataman and Hava Akpinar for their friendship and cooperation and invaluable support.

I would like to thank to all Toppare and Cirpan Research Group members for their friendship.

I appreciate the technical support given by the Central Laboratory.

Finally I would like to thank to my family without whom, this work would never exist.

TABLE OF CONTENTS

ABSTRACT iv

ÖZ vi

ACKNOWLEDGMENTS ix

TABLE OF CONTENTS x

LIST OF TABLES xiv

LIST OF FIGURES xv

LIST OF ABBREVIATIONS xix

CHAPTERS

1 INTRODUCTION 1

1.1 Conjugated Polymers 1

1.1.1 Band Theory 2

1.1.2 Band Gap Engineering 4

1.1.3 Donor Acceptor (DA) Theory 5

1.1.4 Interactions in Conjugated Polymers 6

1.2 Absorption and Emission Processes 8

1.2.1 Emission Pathways of the Excited Molecule 9

1.2.2 Energy Transfer 10

1.2.2.1 Förster Energy Transfer 11

1.2.2.2 Dexter Energy Transfer 11

1.3 Organic Light Emitting Devices 12

1.3.1 Historical Background 12

1.3.2 Advantages 13

Excellent Color Gamut 13

Brightness and Operating Lifetime . . 13
Low Power Consumption 14
Wide Operating Temperature Range . 14
High Contrast under Bright Sunlight . 14
Transparency 14
Thin and Lightweight 14
Ruggedness and Conformability . . . 15
Low Costs 15
1.3.3 Current Use 15
1.3.4 Device Structure 17
1.3.5 Materials Used 17
Indium Tin Oxide (ITO) 17
Cathode Material 18
PEDOT:PSS 18
1.3.6 Working Principle 18
1.4 Aim of the Thesis 20
2 EXPERIMENTAL 21
2.1 Materials 21
2.2 Equipments 21
2.3 Synthesis 22
2.3.1 Synthesis of 4,7-dibromo-4-(tert-butyl)spiro[benzo-[d]imidazole-2,1cyclohexane] 22
2.3.2 Synthesis of 2-Dodecylbenzotriazole 23
2.3.3 Synthesis of 4,7-Dibromo-2-dodecylbenzotriazole . 24
2.3.4 Synthesis of Tributyl(thiophen-2-yl)stannane and Tributyl(4-hexylthiophen-2 yl)stannane 24
2.3.5 Synthesis of 2-Dodecyl-4,7-bis(4-hexylthiophen-2-yl)-2Hbenzo[d][1,2,3]triazole (HTBT) 25
2.3.6 Synthesis of 4,7-Bis(5-bromo-4-hexylthien-2-yl)-2-dodecylbenzo[1,2,3]triazole 26
2.4 Synthesis of the Polymers 26

2.4.1 Synthesis of Poly 4-(biphenyl-4-yl)-4'-tert butyl-spiro[benzo[d]imidazole-2,1'-cyclohexane] (P1) . 26
2.4.2 Synthesis of Poly 4-(biphenyl-4-yl)-2-dodecyl-2H-benzo[d][1,2,3]triazole (P2) 27
2.4.3 Synthesis of Poly(4-(5-(biphenyl-4-yl)-4-hexylthiophen-2-yl)-2-dodecyl-7-(4-hexylthiophen-2-yl)-2H-benzo-[d][1,2,3]triazole (P3) 28
2.5 Physical Properties 28
2.6 Electrochemical Characterization 29
2.6.1 Cyclic Voltammetry 29
2.6.2 Spectroelectrochemistry 30
2.6.3 Kinetic Studies 31
2.7 Optical Characterization 32
2.8 OLED Device Application 32
3 RESULTS AND DISCUSSION 34
3.1 Synthesis 34
3.1.1 Poly 4-(biphenyl-4-yl)-4'-tert-butylspiro[benzo[d]-imidazole-2,1'-cyclohexane] (P1) 35
3.1.2 Poly 4-(biphenyl-4-yl)-2-dodecyl-2H-benzo[d][1,2,3]-triazole (P2) 35
3.1.3 Poly(4-(5-(biphenyl-4-yl)-4-hexylthiophen-2-yl)-2-dodecyl-7-(4-hexyl-thiophen-2-yl)-2H-benzo[d][1,2,3]-triazole (P3) 36
3.2 Electrochemical Properties 37
3.2.1 Cyclic Voltammetry 37
3.2.2 Spectroelectrochemistry 42
3.2.3 Kinetic Studies 44
3.3 Optical Properties 46
3.4 Device performance 50
3.4.1 Energy Transfer Study 53
4 CONCLUSION 61
REFERENCES 63

A APPENDIX A 68
A.1 TGA OF P1 68
A.2 TGA OF P2 69
A.3 TGA OF P3 70
B APPENDIX B 71
B.1 DSC OF P1 71
B.2 DSC OF P2 72
B.3 DSC OF P3 73

LIST OF TABLES

TABLES

Table 3.1 Electrochemical properties of P1, P2 and P3 41
Table 3.2 Kinetic properties of P2 and P3 46
Table 3.3 Optical properties of P1, P2 and P3 50
Table 3.4 OLED performances as a function of varying P3 ratio 59

LIST OF FIGURES

FIGURES

Figure 1.1 Commonly used conjugated polymers 2

Figure 1.2 Band gaps of an insulator, a semiconductor and a metal compared . 3

Figure 1.3 Energy levels of a conjugated polymer in (a) neutral form, with conduction and valence bands only, (b) lightly doped, with the addition of a single bipolaron energy level, and (c) more heavily doped, with a broad bipolaron band 3

Figure 1.4 The formation of polaron and bipolaron defects in a conjugated polymer 4

Figure 1.5 Structural factors affecting the band gap 5

Figure 1.6 Donor (D)-Acceptor(A) Theory 6

Figure 1.7 Entanglement of the chain in poor solvent 7

Figure 1.8 Excitation of a molecule from ground state to various energy levels of first excited state 8

Figure 1.9 Emission of a molecule from excited state to various energy levels of ground state 9

Figure 1.10 The Jablonski Diagram describing the basic photophysical processes: Absorption and Emission 10

Figure 1.11 Förster Energy Transfer 11

Figure 1.12 Dexter Energy Transfer 12

Figure 1.13 Evolution of LED/OLED performance [35] 13

Figure 1.14 a Pioneer display [36] 15

Figure 1.15 Samsung's 2.2" AM-OLED transparent display and 15.5" AM-OLED monitor display [36] 16

Figure 1.16 Philips 13" PolyLED TV prototype demo set-up [37] 16

Figure 1.17 An Indian-bound dual-SIM Android smartphone with a 4.3" (800x480) Super AMOLED display [38] 17

Figure 1.18 The structure of an organic light emitting diode 17

Figure 1.19 Working principle of PLED 19

Figure 2.1 Synthetic route for 4,7-dibromo-4-(tert-butyl)spiro[benzo[d]imidazole-2,1cyclohexane] 22

Figure 2.2 Synthetic route for 2-dodecylbenzotriazole 23

Figure 2.3 Synthetic route for 4,7-dibromo-2-dodecylbenzotriazole 24

Figure 2.4 Synthetic route for stannylation of thiophene and 3-hexyl thiophene 24

Figure 2.5 Synthetic route for 2-Dodecyl-4,7-bis(4-hexylthiophen-2-yl)-2H-benzo[d][1,2,3]triazole (HTBT) 25

Figure 2.6 Synthetic route for 4,7-Bis(5-bromo-4-hexylthien-2-yl)-2-dodecyl-benzo[1,2,3]triazole 26

Figure 2.7 Synthetic route for polymers 27

Figure 2.8 Cyclic voltammetry waveform 29

Figure 2.9 A cyclic voltammogram for a reversible redox process 30

Figure 2.10 Electrode setup 31

Figure 3.1 ^{1}H NMR of Poly 4-(biphenyl-4-yl)-4'-tert-butylspiro[benzo[d]imidazole-2,1'-cyclohexane] (P1) 35

Figure 3.2 ^{1}H NMR of Poly 4-(biphenyl-4-yl)-2-dodecyl-2H-benzo[d][1,2,3]-triazole 36

Figure 3.3 Poly(4-(5-(biphenyl-4-yl)-4-hexylthiophen-2-yl)-2-dodecyl-7-(4-hexylthiophen-2-yl)-2H-benzo[d][1,2,3]triazole (P3). 36

Figure 3.4 Cyclic voltammogram of P1 for both p and n type doping in the presence of 0.1 M $TBAPF_6$/ACN:DCM solution at a scan rate of 50 mV/s . 38

Figure 3.5 Cyclic Voltammogram of P2 for both p and n type doping in the presence of 0.1 M $TBAPF_6$/ACN:DCM solution at a scan rate of 50 mV/s . 39

Figure 3.6 Cyclic voltammogram of P3 for both p and n type doping in the presence of 0.1 M $TBAPF_6$/ACN:DCM solution at a scan rate of 50 mV/s . 40

Figure 3.7 p-Doping electronic absorption spectrum of P1 between 0.0 V and 1.275 V in 0.1 M $TBAPF_6$/ACN:DCM electrolyte-solvent couple (0: neutral state, +: oxidized state) 42

Figure 3.8 p-Doping electronic absorption spectrum of P2 between 0.0 V and 1.275 V in 0.1 M $TBAPF_6$/ACN:DCM electrolyte-solvent couple (0: neutral state, +: oxidized state, -: reduced states) 43

Figure 3.9 p-Doping electronic absorption spectrum of P3 between 0.0 V and 1.275 V in 0.1 M $TBAPF_6$/ACN:DCM electrolyte-solvent couple (0: neutral state, +: oxidized states, -: reduced state) 44

Figure 3.10 Kinetic switching studies of P2 45

Figure 3.11 Kinetic switching studies of P3 45

Figure 3.12 Normalized absorption spectra of P1, P2 and P3 (a): Solution, (b): Thin film 47

Figure 3.13 Normalized emission spectra of P1, P2 and P3 (a): Solution, (b): Thin film 48

Figure 3.14 Normalized absorption and emission spectra of QS in solution . . . 49

Figure 3.15 IVL characteristic of OLED with P3 emissive layer 51

Figure 3.16 Energy levels of the fabricated device 52

Figure 3.17 Electroluminescence and photoluminescence spectra of P3 52

Figure 3.18 Left: Spectral overlap of PVK emission and P3 absorption, Right: energy level diagram of PVK and P3 53

Figure 3.19 Photoluminescence spectrum of all blends as compared with PVK emission 54

Figure 3.20 Luminance versus voltage and current density of 5 % blend device. The inner caption presents the EL and PL spectra 54

Figure 3.21 Luminance versus voltage and current density of 10 % blend device. The inner caption presents the EL and PL spectra 55

Figure 3.22 Luminance versus voltage and current density of 20 % blend device. The inner caption presents the EL and PL spectra 55
Figure 3.23 Luminance versus voltage and current density of 30 % blend device. The inner caption presents the EL and PL spectra 56
Figure 3.24 Luminance versus voltage and current density of 40 % blend device. The inner caption presents the EL and PL spectra 56
Figure 3.25 The luminance efficiencies of all polymer blends 58
Figure 3.26 The CIE choramaticity diagram of all blends 59

Figure A.1 TGA result of P1 68
Figure A.2 TGA result of P2 69
Figure A.3 TGA result of P3 70

Figure B.1 DSC result of P1 71
Figure B.2 DSC result of P2 72
Figure B.3 DSC result of P3 73

LIST OF ABBREVIATIONS

ACN	Acetonitrile
BIm	Benzimidiazole
BTz	Benzotriazole
CB	Conduction band
CP	Conjugated Polymer
CV	Cyclic Voltammetry
DA	Donor Acceptor
DSC	Differential Scanning Calorimetry
E_g	Band Gap Energy
ECDs	Electrochromic Device
EL	Electroluminescence
HOMO	Highest Occupied Molecular Orbital
HTBT	2-Dodecyl-4,7-bis(4-hexylthiophen-2-yl)2Hbenzo[d][1,2,3]triazole
ITO	Indium Tin Oxide
LUMO	Lowest Unoccupied Molecular Orbital
NHE	Normal Hydrogen Electrode
NMR	Nuclear Magnetic Resonance
OFETs	Organic Field Effect Transistors
OLEDs	Organic Light Emitting Diodes
PA	Polyacetylene

PEDOT:PSS	Poly(3,4-ethylenedioxythiophene):poly(styrenesulfonate)
PL	Photoluminescence
PLED	Polymer Light Emitting Diode
$TBAPF_6$	Tetrabutylammonium hexafluorophosphate
TGA	Thermal Gravimetric Analysis
VB	Valance Band

CHAPTER 1

INTRODUCTION

1.1 Conjugated Polymers

Polymers have been considered as insulators for a long time. However this assumption was denied with the discovery of the electrical conductivity of polyacetylene [1] which led Heeger, MacDiarmid and Shirakawa to achieve a Nobel Prize in 2000 [2]. After this, conducting polymers received great interest of the researchers.

Conjugated polymers usually have carbon atoms in a series of alternating single and double bonds along the length of the polymer backbone. This enables delocalization of the electrons along the backbone of the structure. Energy needed to move an electron from the Highest Occupied Molecular Orbital (HOMO) to the Lowest Unoccupied Molecular Orbital (LUMO) of the conjugated unit is decreased by extended delocalization. Therefore, the photons can be absorbed and emitted in the visible spectrum of light which is in the range of 400 - 700 nm. Thus, these polymers become available for applications such as organic light emitting devices and polymer based solar cells [3–6]. Some of the examples of commonly used conjugated polymers are shown in Figure 1.1.

Conjugated polymers became a focusing subject of future technology research since it is possible to employ them in flexible display devices [7].

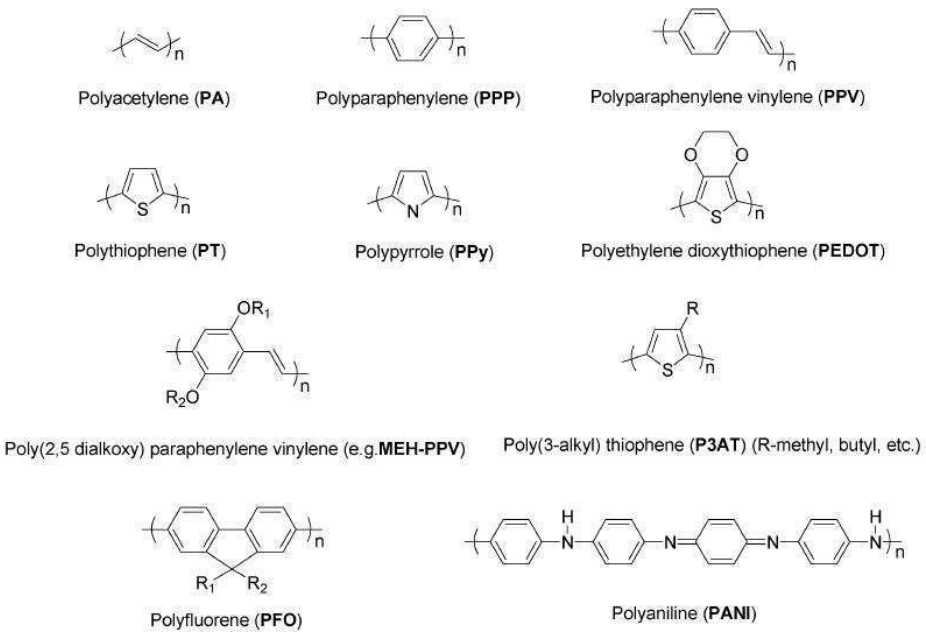

Figure 1.1: Commonly used conjugated polymers

1.1.1 Band Theory

The Band Theory investigates the electrical behaviours of conductors, semiconductors and insulators. Regarding the theory, the valance band is occupied with electrons while the conduction band is unocuppied . These are separated by an energy gap where no intermediate energy levels are present. The electrons can migrate from valance band to the conduction band via excitation of electrons by a thermal or a photochemical process. Therefore, conductors, in which the conduction and valance bands are overlapped, are able to conduct electricity by mobile electrons. In contrast, insulators can not conduct electricity because of their high band gaps, which result from the large energy difference between their conduction and valance bands. Whereas the moderate band gap of semiconductors can be modified to enable conductivity by doping process. By this modification conduction of electricity is enabled in semiconductors [8]. Band gaps of insulators, semiconductors and metals are compared in Figure 1.2.

Conductivity in conjugated polymers occurs in a similar way to semiconductors. Conjugated polymers reveal an energy gap (E_g) between the HOMO and the LUMO. The energy gap of the polymer can be changed following electrical or chemical doping

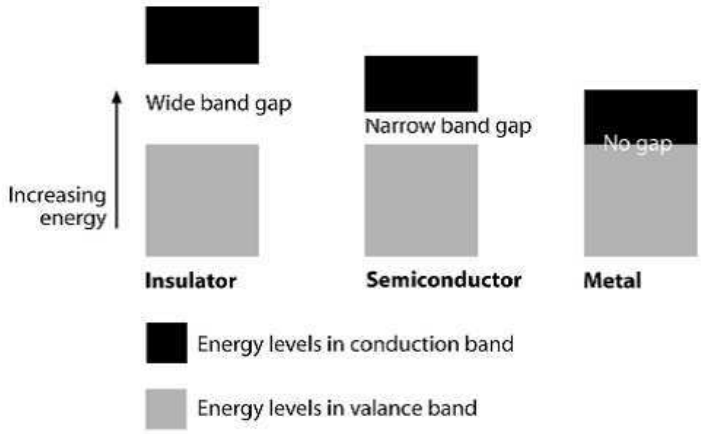

Figure 1.2: Band gaps of an insulator, a semiconductor and a metal compared

processes. These changes cause formation of polarons and bipolarons which are intra-band transitions with lower energy and charge carriers respectively. This results in an increase in electrical conductivity and optical property of the polymer [8, 9].

Energy levels of a conjugated polymer in neutral, lightly doped and heavily doped form is given in Figure 1.3

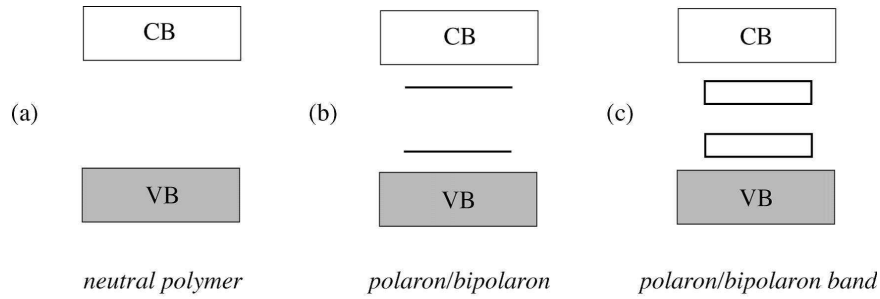

Figure 1.3: Energy levels of a conjugated polymer in (a) neutral form, with conduction and valence bands only, (b) lightly doped, with the addition of a single bipolaron energy level, and (c) more heavily doped, with a broad bipolaron band

The resulting defect is called a negative or a positive polaron in case of a reduction or an oxidaton of one of the π orbitals respectively. Moreover, it is called a bipolaron if the defect occurs at both sites. An example configuration of polarons and bipolarons is given in Figure 1.4

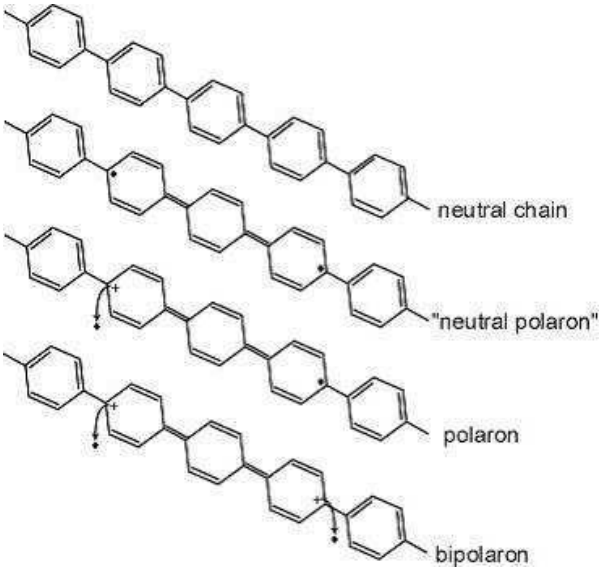

Figure 1.4: The formation of polaron and bipolaron defects in a conjugated polymer

1.1.2 Band Gap Engineering

In order to suit optoelectronic applications such as transistors, LEDs, electrochromic devices and solar cells; it is necessary to control the band gap of the π conjugated polymers. Moreover, for the electronic and photonic applications, these active materials must reveal some properties such as appropriate HOMO/LUMO energy levels, absorption and emission and charge carrier properties.

Band gap of aforementioned type of polymers is controlled by five factors and can be expressed by Equation 1.1 [10].

$$E_g = E_{BLA} + E_{Res} + E_{Sub} + E_u + E_{Int} \tag{1.1}$$

In Equation 1.1, E_{BLA} stands for the bond length alternation. Synthetic methods can be employed to increase and reduce the band gap of the resulting polymer which results in Bond Length Alternation (BLA). Resonance effect is denoted by E_{Res}. Those polymers are restricted to be in two forms which are aromatic and quinoid according to their non-degenerate ground states. In general, the aromatic form reveals higher band gap through higher stabilization energy.

The substituent effect is represented by E_{Sub}. The HOMO/LUMO energy levels can be changed by the incorporation of electron deficient and electron rich groups. HOMO level is increased by electron donating groups and LUMO level is decreased by electron withdrawing groups. The dihedral angle between consecutive units is denoted by E_u. This parameter increases the band gap by limiting the delocalization of π electrons along the chain. The aforementioned four factors given in Equation 1.1 govern which synthetic approach should be employed for the molecular engineering of the HOMO/LUMO of an isolated system. Inter-chain effects are denoted by E_{Int}. This parameter comes into play when the polymer chains or individual molecules assemble into a material (Figure 1.5).

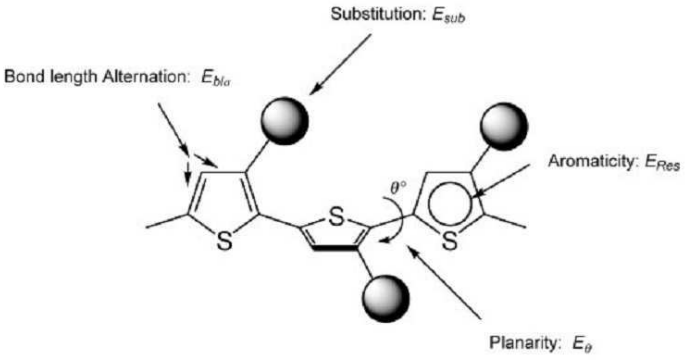

Figure 1.5: Structural factors affecting the band gap

Several synthetic approaches exist to alter the band gap of a polymer. Among these, the Donor-Acceptor Theory has been one of the popular choices.

1.1.3 Donor Acceptor (DA) Theory

The Donor-Acceptor theory has been widely used for tailoring the band gap of resulting conjugated polymer. It is accomplished by substitution of an electron rich donor to an electron poor acceptor unit. Thus intermolecular charge transfer is enabled [11–13].

Electronic and optoelectronic properties can be modified by the hybridization of the HOMO of the donor and the LUMO of the acceptor in which a stronger double bond

character between the donor and acceptor units is enabled. Desired properties can be achieved by an appropriate match of these groups. It is possible to have lower band gap by combining the high level of HOMO property of the donor and low level of LUMO property of the acceptor in the same polymer. Thus the resulting polymer reveals an ionization potential closer to the donor and an electron affinity closer to the acceptor by the help of hybridization between the high level of the HOMO of the donor and the low level of the LUMO of the acceptor (Figure 1.6) [14].

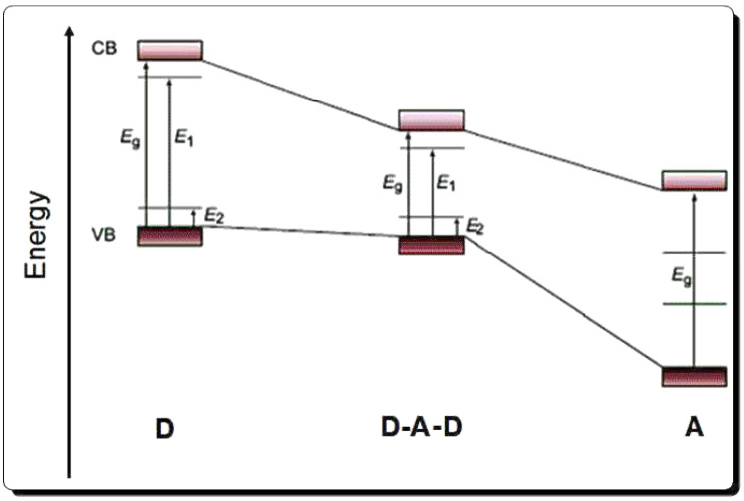

Figure 1.6: Donor (D)-Acceptor(A) Theory

The implementation of donor-acceptor type conjugated polymers gains popularity because of the fact that these type of polymers enables adjusting of optical properties by the help of structural modifications [15]. In addition to the discussed effects that contribute to spectral property of the polymer, global parameters such as interactions in conjugated polymers needs to be investigated.

1.1.4 Interactions in Conjugated Polymers

The photophysical properties of conjugated polymers are usually affected by structure of the polymer and whether being in solution or film. Excited state species are limited to a single chain in a good solvent such as molecular solutions. In contrast, the π bands of neighboring polymer chains in entangled forms (Figure 1.7) may overlap which induces inter-chain species such as aggregates in films (i.e. poor solvent con-

ditions). These aggregates are regarded as various species that reveal spectroscopic characteristics that is related to a range of phenomena resulting from close contact between two molecules. Examples include π-stacking, interactions between transition dipoles, excimers and exciplexes [1] [16–18].

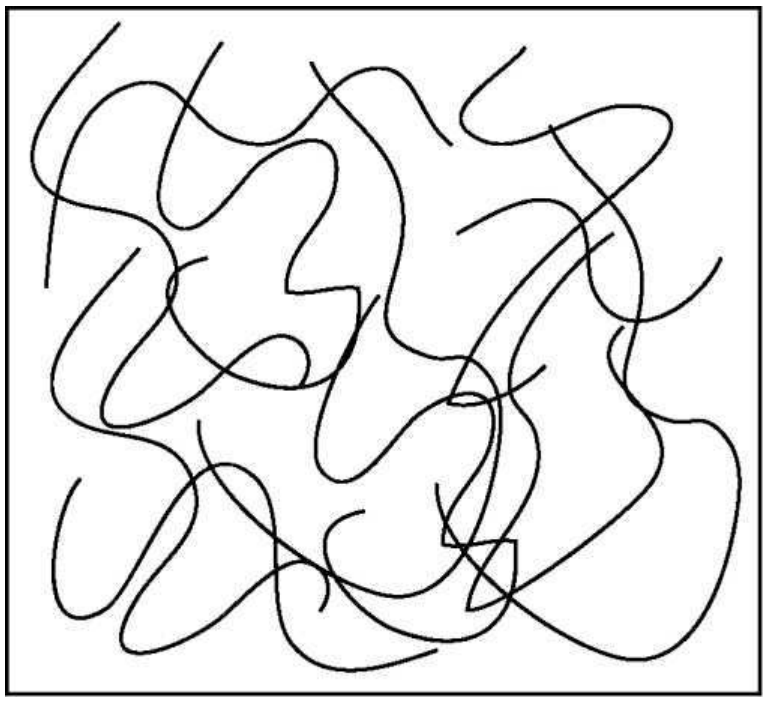

Figure 1.7: Entanglement of the chain in poor solvent

Aggregate species reveal an important impact on the determination of photophysical properties of conjugated polymers. These excited species delocalize over a larger number of atoms or chromophores which yield red shifted emission. Moreover, by the help of the flexibility of these polymers, aggregates can be formed between different polymer chains (inter-chain aggregates) [20, 21] and between different overlapping segments of the same polymer chain (intra-chain aggregates) [22, 23].

The impact of various solvent properties such as temperature, quality and concentration as well as the chemical properties of the polymer such as backbone type, side chains, heteroatoms and heterogeneity on optical properties have been investigated for various conditions. For instance, concentration in a solution or gel phase, or cast-

[1] Excimers are formed by the interaction of two molecules of the same kind, where one molecule is in the electronically excited state and the other is in its ground state. On the other hand, exciplexes are formed by the interactions of two molecules of different kind [19].

ing properties in films affects the photophysical properties such as quantum yield, emission wavelength and carrier mobility [20, 24]. The quality of the solvent is governed by solvent polarity, temperature and polymer concentration. For instance, good solvents yield an open structure in the polymer which reduces energy transfer whereas poor quality of the solvent reveals gelation and inter-chain aggregation.

1.2 Absorption and Emission Processes

A molecule can be excited by absorption of a photon or a phonon, by dipole-dipole interactions with a neighboring molecule, or by injecting electrical charges.

When a molecule absorbs light, one of its valence electrons is promoted to the higher energy level. The energy of light needed for such transition gives information about the energy difference between these states. The energy gaps between 1 eV and 4 eV allows the absorption and emission of photons in the visible range.

Absorption of the photon increases the energy of the molecule and promotes it to a photo excited state. The molecule is now energetically unstable and dissipates the excess energy as soon as possible by thermally, by chemically or by emitting photon. After the absorption process, the molecule can be excited to one of the several vibrational levels within the S_1 state depending on the absorbed energy (Figure 1.8). When this occurs, the excess vibrational energy is lost as heat to the surroundings and goes to the lowest vibrational energy level of S_1. After this relaxation, the molecule can relax to one of the several vibrational state of S_0 (Figure 1.9).

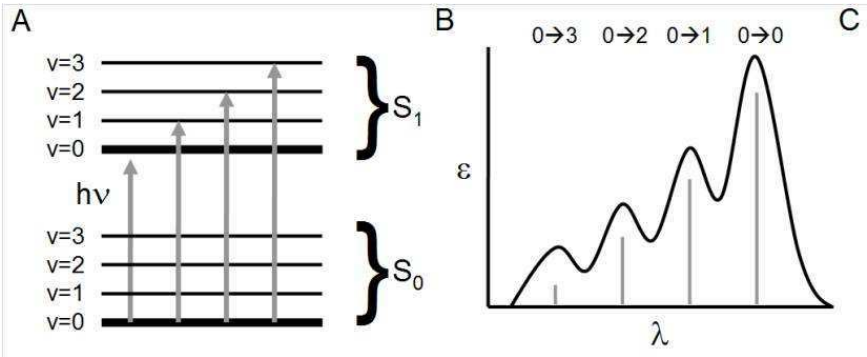

Figure 1.8: Excitation of a molecule from ground state to various energy levels of first excited state

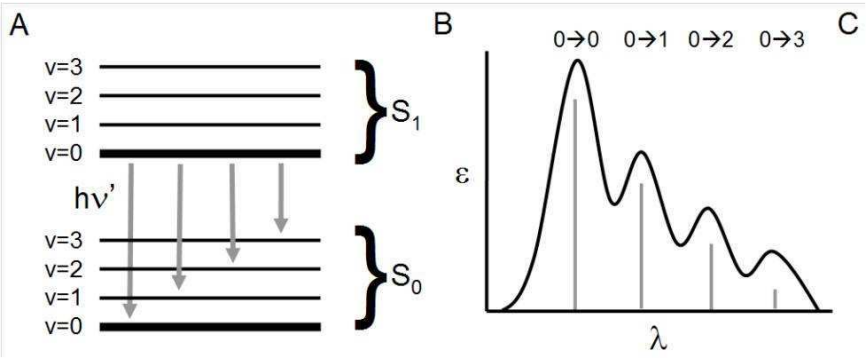

Figure 1.9: Emission of a molecule from excited state to various energy levels of ground state

1.2.1 Emission Pathways of the Excited Molecule

Once a molecule is in its excited state, four possible processes can occur namely fluorescence, phosphorescence, nonradiative relaxation or dissociative bond breaking [25] (Figure 1.10).

Radiative decay involves deactivation of an excited state by emitting a photon [26]. Fluorescence and phosphorescence are the types of radiative decay. Fluorescence occurs faster as it is spin allowed which means that the transition between two states of the same spin is enabled. Whereas, the phosphorescence necessitate the transition between two states of different spin [6]. As can be seen from the Figure 1.10, fluorescence always occurs at a higher energy than the phosphorescence which results in shorter wavelength emission.

Nonradiative transitions involve all the pathways of deactivation of the excited state without emitting light [27]. The energy is lost by collision with other molecules. If this transition occurs between the two states of the same spin, the process is called as internal conversion. On the other hand, the process is called as inter-system crossing, if the transition occurs between the states with different spins.

The fluorescence occurs with a lower energy than absorption due to energy loss by vibrational relaxations or nonradiative relaxations explained above. The energy difference between absorption and fluorescence spectra is called as Stoke's shift which is an indication of singlet excited state distortion.

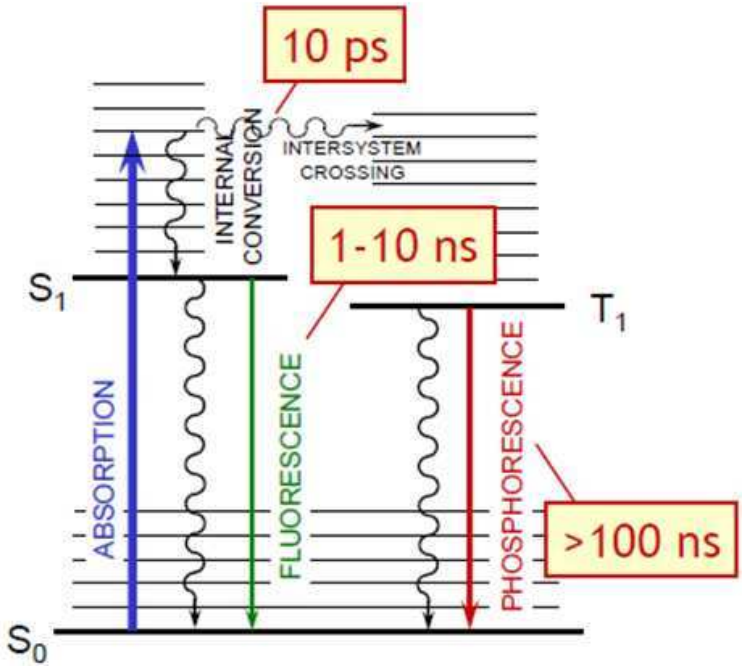

Figure 1.10: The Jablonski Diagram describing the basic photophysical processes: Absorption and Emission

The fluorescence quantum yield is a measure of the probability of absorbed photon that will result in emission. The spectral overlap between absorption and emission and Stoke's shift are important parameters that define the energy loss and contribution to fluorescence quantum yield decrease.

1.2.2 Energy Transfer

In addition to the relaxation methods explained previously; excited molecules can transfer energy and electrical charge to neighboring molecules by various ways, depending on the distance between donor and acceptor according to Equation 1.2.

$$\begin{aligned} D + h\nu &\rightarrow D^* \\ D^* + A &\rightarrow D + A^* \end{aligned} \tag{1.2}$$

The basic requirements for an energy transfer are:

1. The energy of D must be higher than the energy of A

2. The energy transfer process must be faster than the lifetime of D^*

1.2.2.1 Förster Energy Transfer

For the Förster Energy Transfer, overlap of the emission spectrum of D^* with the absorption spectrum of A is necessary. It can be seen that the electron systems of D^* and A are analogous to the coupled mechanical oscillators. Therefore, the excitation energy is shared through resonance if one of the electrons is excited (Figure 1.11 [28]). Because of its electrostatic character, Förster Energy Transfer can occur over relatively long distances such as (30-100 A^o). Moreover, the process is said to occur very rapidly (10^{-9} s).

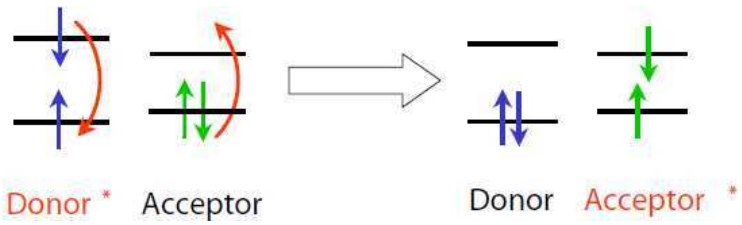

Figure 1.11: Förster Energy Transfer

This energy transfer mechanism is preferred provided that emission by the D^* and the absorption by A are allowed transitions. Therefore, the S-S energy transfer is enabled by this mechanism whereas T-T transition is not. The probability of dipole-dipole energy transfer is proportional to $1/r^6$ (where r is defined as the distance between the donor and the acceptor).

1.2.2.2 Dexter Energy Transfer

Another type of energy transfer which is nonradiative is the so called Dexter Energy Transfer. In contrast to Förster Energy Transfer, a molecule can be excited by the diffusion of exciton from D^* to A (Figure 1.12). This is accomplished by transferring an electron and a hole at the same time [29].

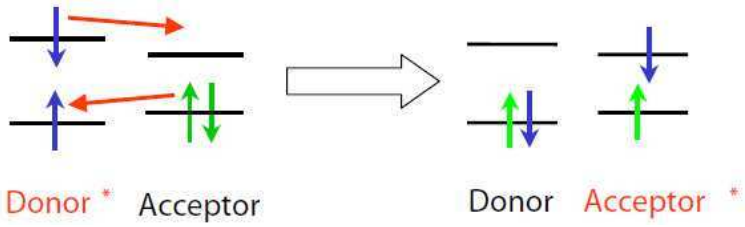

Figure 1.12: Dexter Energy Transfer

As the rate of energy transfer is proportional to the overlapping of molecular orbitals, this type of energy transfer occurs if the molecules are close enough (i.e. 10-15 A^o) [30]. This energy transfer mechanism allows both of the S-S and T-T energy transfer processes to occur, in contrast to Förster Energy Transfer.

1.3 Organic Light Emitting Devices

1.3.1 Historical Background

Electroluminescence (EL) is the process in which the recombination of an electron and a hole, which are injected by an external electrical field, creates an excited molecule that emits photons upon relaxation to the ground state. This phenomena is first observed by Helfrich and Schneider [31] when they applied external voltage using electrodes on single crystals of anthracene. Later, during the late 80s, Tang and vanSlyke [32], and Adachi et al [33] separately developed operational OLEDs by the help of organic dyes. Requirement of voltages were lower and produced light was brighter than the findings from the previous research. Electroluminescence in conjugated polymers was reported by Burroughes et al [34] in 1990. Under the light of these key discoveries, concentrated research on commercial applications of OLEDs has been increased. Evolution of LED/OLED performance through the past years is reported by Sheats et al [35] (Figure 1.13).

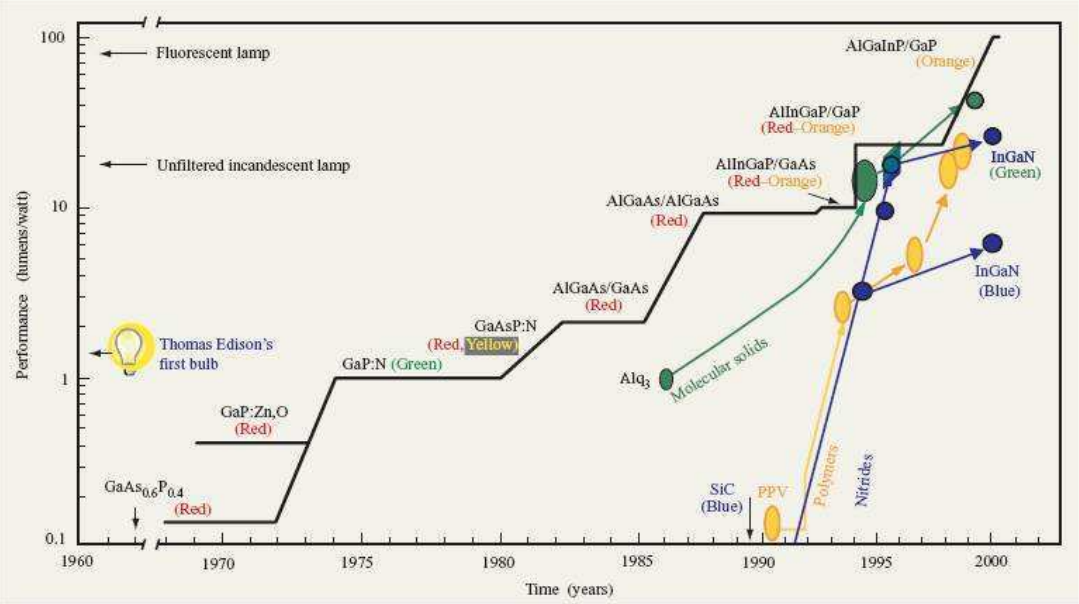

Figure 1.13: Evolution of LED/OLED performance [35]

1.3.2 Advantages

Excellent Color Gamut The variety of organic materials employed in the structure of OLED can be used to tailor the colors emitted. The primary focus on OLED research nowadays is to develop full-color OLEDs (red, green and blue) that have a long life-span and are power efficient. In this manner, the huge variety of organic structures provide the ability to meet custom color requirements of the community.

Brightness and Operating Lifetime As the OLEDs are operated under current, the brightness can be adjusted in a very wide dynamic range. They can be used at very high brightness levels such as > 100.000 cd/m^2 and very low brightness levels such as 1 cd/m^2 uniformly without flicker. However, the life spans of these devices are inversely proportional to brightness, therefore they are typically specified to be used at moderate levels. Commonly reported lifetimes are in the range 5000-10000 hours at 100 cd/m^2. Research on improved materials for both increased brightness and longer life span has been in progress.

Low Power Consumption As the OLED displays are operated by current, the active matrix architectures are significantly more power efficient comparing to the simple passive matrix architectures. For instance, simulations of an IMT-2000 full-color cell phone display (app. 2" diag) reveal that a PM-OLED with a 50 % efficient circular polarizer and 30 % illuminated consumes about 250 mW at 100 cd/m^2 while an AM-OLED is operated about 110 mW. The use of phosphorescent materials in an AM-OLED further decreases consumption to about 65 mW.

Wide Operating Temperature Range LCD displays are affected by the cold and necessitate the heating of the backside. In contrast, OLED displays operate very well at very low temperatures.

At high temperatures, LCDs can lose their light twisting properties. Although OLEDs have some limitations due to the glass transition temperature (T_g) of the employed organic materials, commonly reported materials reveal a T_g in the range 90 - 95 °C with a stable operating temperature of 70 °C.

High Contrast under Bright Sunlight The displays are operated at extremely bright levels so as to obtain reasonable viewability under direct sunlight. It is preferable to improve the contrast because of the fact that human eye is more sensitive to contrast rather than brightness. Therefore, the display reflectivity must be optimized. As the OLEDs emit light themselves, they provide a very good contrast.

Transparency As the OLED can be fabricated on a transparent substrate, transparent OLEDs can be produced. For instance, Samsung introduced the concept of transparent OLED TV. Future uses may include head up displays for automotive windshields.

Thin and Lightweight As they possess a very thin profile, OLEDs can be integrated to any environent that dictate limited space. For instance, profile of a typical poly-Si AM-LCD is 6 mm and a VFD 16-20 mm while an OLED fabricated on an 0.7

mm glass yields a profile less than 1.4 mm. Moreover, research by UDC is concentrated on fabricating OLED on flexible substrates such as 0.18 mm thick PET film.

Ruggedness and Conformability It can be evaluated that the flexible OLEDs are more immune to breakage and are more rugged. These OLEDs are insensitive to compression and vibration as they are monolithic and constructed in a solid state, in contrast to LCDs, which are produced with cell gaps that create distorted images from contact pressure and cell spacers that can displace with excessive vibration. For instance, flexible OLEDs have been shown to bend to a radius of curvature of < 1 cm.

Low Costs OLED technology promises a significant cost reduction when compared to LCD technology. The reduction in cost mainly arises from the production, for which fewer processing steps will be employed. Moreover current LCD infrastructure can be used with few modifications. Also further developments such as roll-to-roll processing for flexible OLEDs will reduce the cost and maintain mass production.

1.3.3 Current Use

The first OLED, a glass-based 256 x 64 pixel display for an automotive radio console, was introduced by Pioneer Electronic Corporation in 1997 [36] (Figure 1.14).

Figure 1.14: a Pioneer display [36]

In 2003, Samsung demonstrated 2.2" AM-OLED and 15.5" AM-OLED monitor display [36] (see Figure 1.15).

Phillips also demonstrated the first PLED TV screen [37] (see Figure 1.16).

State of the art uses in commercial products include mobile phones (Mixromax Pixel A90 (see Figure 1.17 [38]), BLU Vivo 4.3, Toshiba T-02D, Samsung Exhilarate, Sam-

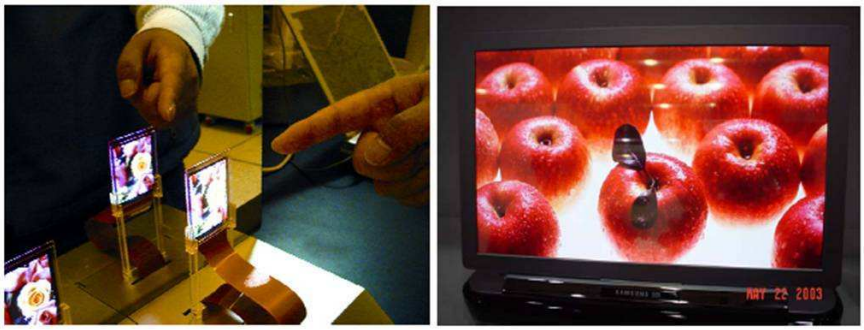

Figure 1.15: Samsung's 2.2" AM-OLED transparent display and 15.5" AM-OLED monitor display [36]

Figure 1.16: Philips 13" PolyLED TV prototype demo set-up [37]

sung Galaxy R style, Oppo Finder, Samsung Omnia M), digital cameras (Samsung MV900F, Samsung EX2F, Olympus Tough TG-1 iHS, Samsung NX210, Samsung NX20, Sony DSC-TX66, Olympus OM-D E-M5), A/V players (Cowon D3 Plenue, Sony NW-A850, Cowon J3, INS Mobile iVIDI, Cydle P29H, Samsung IceTouch, Viliv P3), OLED TVs (Samsung ES9500, LG 55EM9600, Sony BVM-F250/F170, Sony PVM-1741 / PVM-2541, Sony BVM-E250 / BVM-E170, LG EL9500 OLED TV, SonyDrive XEL-1 OLED TV), OLED lamps (Vela OLED Chandelier, Vela OLED wall sconce, Cinimod Studio OLED Moon chandelier, Liternity victory, Blackbody smart oled, Lumiotec Hanger, Lumiotec Vanity) and a variety of other devices such as wrist watches, headsets, car audio systems, remote controllers, digital photo frames and many kinds of devices.

Figure 1.17: An Indian-bound dual-SIM Android smartphone with a 4.3” (800x480) Super AMOLED display [38]

1.3.4 Device Structure

A typical single-layer polymer OLED is presented in Figure 1.18. A thin polymer film is spin-coated from solution on a transparent bottom electrode, usually Indium-Tin-Oxide (ITO) coated glass/plastic, which forms the anode. A low work-function metal (calcium or barium) is evaporated on top of the polymer and serves as cathode.

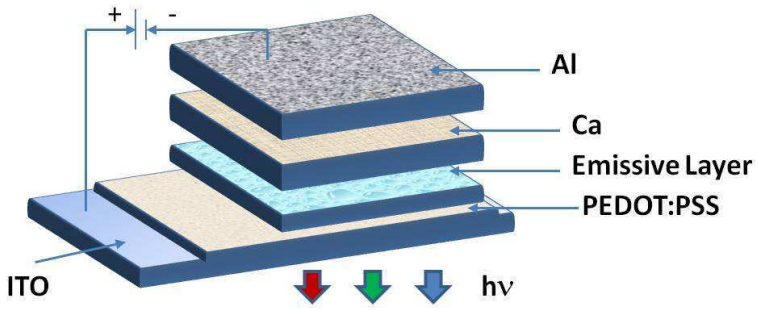

Figure 1.18: The structure of an organic light emitting diode

1.3.5 Materials Used

Indium Tin Oxide (ITO) Commonly used as the transparent and hole injecting contact (anode) is ITO. The material is transparent, conductive and has a reasonably high work function (4.5 to 5 eV). Indium oxide (In_2O_3) is a wide band-gap semiconductor [39]. To modify the conductivity of the material, indium oxide is degenerately

doped with tin. To obtain films, In_2O_3 and SnO_2 are usually simultaneously sputtered onto transparent substrates such as glass in a molar ratio of 91 % : 9 %. Because ITO is non-stoichiometric, the electronic properties depend on the preparation and cleaning processes used. An oxygen plasma treatment can increase the work function by as much as 0.5 eV and thus increase the efficiency of the device.

Cathode Material The material used as a cathode should have a low work function like alkali metals for good electron-injecting properties. However, all of these metals such calcium are prone to reactions with either the emissive material or with the surrounding atmosphere leading to device degradation. The device stability can be enhanced by using alloys containing these metals in a matrix of more stable metals like silver or aluminum.

PEDOT:PSS PEDOT:PSS can be used as transparent anode, beside this it is used for the purpose of hole transporting layer. It improves the surface roughness of ITO and qualifies film morphology. Furthermore PEDOT:PSS has very limited solubility in common organic solvents which enables the spin coating of polymer solutions on it [40].

1.3.6 Working Principle

The operation principles of organic light emitting diodes include four steps namely: charge carrier injection, charge carrier transport, carrier recombination, emission process which are depicted in Figure 1.19.

Single layer OLEDs are dual carrier thin film devices. Under forward bias electrons are injected from metal to LUMO of the electroluminescent polymer while holes are injected from low work function electrode to HOMO of the polymer.

Ideally, the work function of the cathode should match with the LUMO energy level of the polymer and also the work function of the anode should perfectly match with the HOMO of the polymer.

When the work functions of the contacts between electrodes and polymer do not

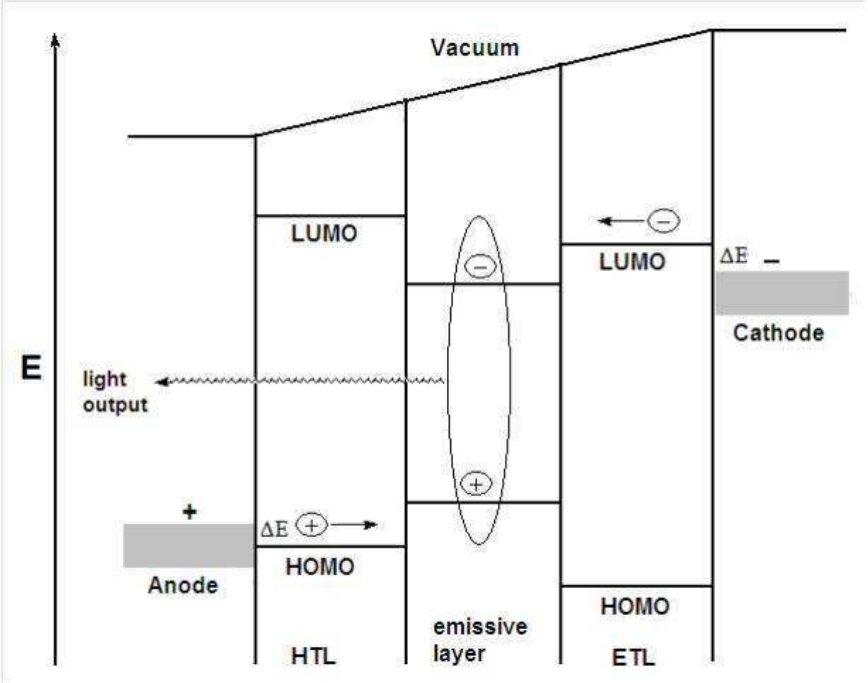

Figure 1.19: Working principle of PLED

match, energy barriers are formed at the respective interfaces. The height of the barrier for hole injection is determined by the difference between HOMO of the polymer and work function of anode. The height of the barrier for electron injection is determined by the difference between work functions of the cathode and LUMO of the polymer. When electrical field is started to apply, the barrier energies are overcomed and injection of carriers take place. However the existence of disorder in organic semiconductors adds an obstacle to the injected carriers [41, 42]. Due to disorder, a distribution of site energies is created, and injected carriers occupy the molecular sites in contact with electrodes or low-energy end of the distribution. To move further into the organic materials, the carriers must overcome random energy barriers which force most of the injected carriers to back flow into the electrode at low applied field strength. Back flow is avoided when the electrical field is increased. Thus the efficiency of injection into organic materials is enhanced.

After the injection is accomplished, the transport of the charges can be seen as a hopping process [43, 44] that is based on an electron-transfer reaction, in which an electron is moving between two neighboring molecules [45].

The charges in the bulk are in coulombic interaction. They reveal opposite spin rates which creates singlet excitons in the recombination zone [46]. Light is emitted as these excitons decay to the ground state radiatively. However, some charges are unable to relax. So both carriers might travel in the opposite directions through the material under the influence of external electrical field. Hence, light would not be emitted from those carriers. Ideally same amount of electrons and holes should be injected in which the choice of materials is an important part of the ”balanced injection” concept. Probability of the radiative emission is increased by the balanced injection [35].

In fluorescent electroluminescence, emission is limited to singlet excitons in contrast to fluorescence. Because of this, electroluminescence efficiency which is governed by emitted photons per injected electron is less than 25 % for fluorescent materials [47]. Photoluminscence efficiency could be unity theoretically as all the electron-hole pairs form singlet excitons [47].

1.4 Aim of the Thesis

The aim of this thesis is to emphasize the applicability of biphenyl based conjugated polymers in light emitting devices. Biphenyl is selected as the based polymer regarding its excellent thermal and spectral properties. The well known Donor-Acceptor Theory is used to establish the synthetic pathway for the structural modifications in order to tune the spectral properties. Solubility issues regarding this polymer is solved by copolymerizing with soluble units. For this purpose; poly 4-(biphenyl-4-yl)-4’-tert butylspiro[benzo[d]imidazole-2,1’-cyclohexane] (P1), poly 4-(biphenyl-4-yl)-2-dodecyl-2H-benzo[d][1,2,3]triazole (P2) and poly(4-(5-(biphenyl-4-yl)-4-hexylthiophen-2-yl)-2-dodecyl-7-(4-hexylthiophen-2-yl)-2H-benzo[d][1,2,3]triazole (P3) are synthetized using Suzuki coupling process. It is observed that the emission color of biphenyl is tuned from blue to orange.

CHAPTER 2

EXPERIMENTAL

2.1 Materials

All chemicals were purchased from commercial sources and used without further purification unless otherwise mentioned. Dichloromethane (DCM) (Aldrich), chloroform ($CHCl_3$) (Aldrich), ethanol (Aldrich), HBr (Merck), acetonitrile (ACN) (Merck), methanol (Merck), tributyl tin chloride (Aldrich), N-butyl lithium (Aldrich), thiophene (Merck), 3-hexyl thiophene (Aldrich) and $MgSO_4$ (Aldrich), polyvinylcarbazole (Aldrich) , quinine sulfate (Aldrich) were used without further purification. THF (Fisher) was used after distillation with benzophenone (Merk) and sodium. Tetrabutylammonium hexafluorophosphate ($TBAPF_6$) (Aldrich), PEDOT:PSS (H.C. Stark) were used as received. ITO were supplied by Visiontek Systems Ltd., Al and Ca was taken from Kurt J. Lesker.

2.2 Equipments

^{1}H-NMR and spectra of the polymers were recorded in $CDCl_3$ on Bruker Spectrospin Avance DPX-400 Spectrometer. Chemical shifts were given in ppm downfield from tetramethylsilane (TMS). Column chromatography of products was performed using Merck Silica Gel 60 (particle size: 0.040-0.063 mm, 230-400 mesh ASTM). Average molecular weights were determined by gel permeation chromatography (GPC) using a Polymer Laboratories GPC 220 in tetrahydrofuran (THF).Thermal analysis of the polymers were conducted by Perkin Elmer diamond differential scanning calorimetry

(DSC) in nitrogen environment, in a 25-250 °C temperature range with 10 °C /min measurements and Perkin Elmer Pyris 1 thermal gravimetric analysis (TGA) in nitrogen environment, in a 25-700 °C temperature range with 10 °C /min measurements.

All electrochemical studies were performed in a three-electrode cell consisting of an ITO as the working electrode, platinum (Pt) as the counter electrode, and Ag wire as the reference electrode using a Voltalab 50 potentiostat at ambient conditions.The value of Normal Hydrogen Electrode (NHE) was taken as -4.75 eV.

Spectroelectrochemical studies of the polymers were directed by Varian Cary 5000 UV-Vis spectrophotometry. Fluorescence measurement were conducted by Varian Eclipse spectrofluorometer.

2.3 Synthesis

2.3.1 Synthesis of 4,7-dibromo-4-(tert-butyl)spiro[benzo[d]imidazole-2,1cyclohexane]

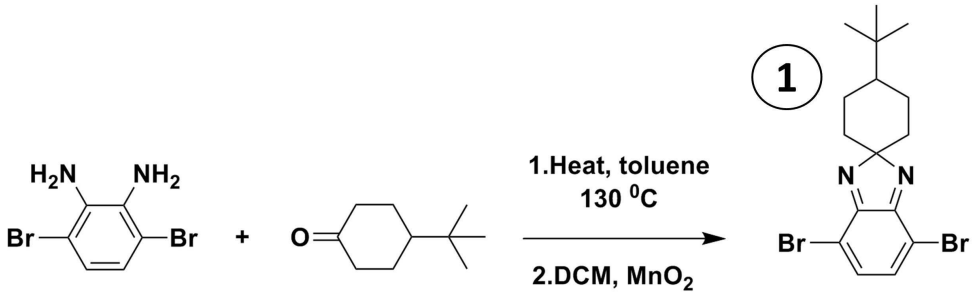

Figure 2.1: Synthetic route for 4,7-dibromo-4-(tert-butyl)spiro[benzo[d]imidazole-2,1cyclohexane]

To a three-necked round bottom flask were added 3,6-dibromobenzene-1,2-diamine (300 mg, 1.13 mmole), 4-tert-butylcyclohexanone (174 mg, 1.13 mmole). The flask was flushed with argon and 8 ml toluene was added and the mixture stirred at 130 °C for 24 h. Then the solvent was removed under reduced pressure. The crude product was dissolved in 11 ml dichloromethane and stirred at room temperature under argon atmosphere. To this solution, 85 % activated manganese (IV) oxide (800 mg, 9.16 mmole) was added. After stirring at room temperature for 4 h, the reaction mixture

was filtered, diluted with dichloromethane (80 ml), washed with distilled water (3 x 80 ml) and dried over $MgSO_4$. After removing the solvent under reduced pressure, the residue was purified by column chromatography using hexane:ethylacetate (10:1) as the eluent. 4,7-Dibromo-4-(tert-butyl)spiro[benzo[d]imidazole-2,1-cyclohexane] was obtained as a yellow solid with a yield of 55 %. ^{1}H NMR (400MHz, $CDCl_3$): δ (ppm) 7.12 (s, 2H), 2.25 (t, 2H), 2.10 (m, 1H), 1.70 (t, 2H), 1.60 (t, 2H), 1.30 (t, 2H), 0.90 (s, 9H). ^{1}3C NMR (100MHz, $CDCl_3$): δ (ppm) 157.00, 156.70, 135.80, 135.60, 119.30, 107.50, 107.50, 107.45, 47.80, 47.85, 47.80, 32.50, 35.80, 35.75, 27.75, 25.7.

2.3.2 Synthesis of 2-Dodecylbenzotriazole

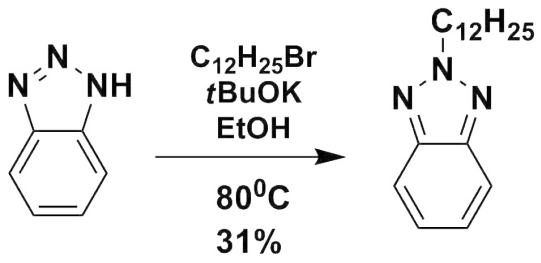

Figure 2.2: Synthetic route for 2-dodecylbenzotriazole

Alkylated benzotriazole was previously published [48]. To a three-necked flask were added 1,2,3-benzotriazole (5.0 g, 42 mmole), potassium tert-butoxide (5.0 g, 44 mmole), and bromododecane (12.2 g, 49 mmole). The flask was flushed with argon and 50 ml of ethanol was added.The mixture was refluxed for 12 h monitored by TLC. After evaporation of the solvent, the residue was dissolved in $CHCl_3$ and extracted with water. $MgSO_4$ was used to dry the organic extract. Then the solvent was evaporated under reduced pressure. The residue was subjected to column chromatography (3:2 chloroform:hexane) to obtain 2-dodecylbenzotriazole as a colorless oil(3.7 g, 31 %) ^{1}H NMR (400MHz, $CDCl_3$, δ): 7.76 (m, 2H), 7.26 (m, 2H), 4.62 (t, J=7.1Hz 2H), 2.12 (m, 2H), 1.25-1.15 (m, 18H), 0.78 (t, J=6.0 Hz, 3H); ^{13}C NMR (100MHz, $CDCl_3$, δ): 144.3, 126.1, 117.9, 56.6, 31.8, 30.0, 29.5, 29.4, 29.4, 29.3, 29.3, 29.0, 26.5, 22.6, 14.0.

2.3.3 Synthesis of 4,7-Dibromo-2-dodecylbenzotriazole

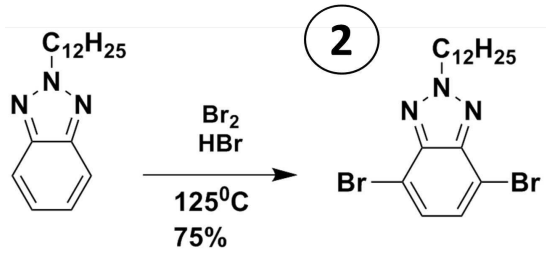

Figure 2.3: Synthetic route for 4,7-dibromo-2-dodecylbenzotriazole

To a three-necked round bottom flask were added 3.7 grams of 2-dodecylbenzotriazole (13.1 mmole) and 15 ml of HBr (47 %). Reaction mixture was heated at 100 °C with stirring for 1 h. After addition of 5.9 grams of bromine (36 mmole), it was refluxed for 12 hours at 135 °C. The reaction was monitored by TLC. After the reaction was ended, the mixture was treated with $NaHCO_3$ solution to get rid of excess Br_2. The residue was extracted with dichloromethane and brine. The combined organic layers were dried over $MgSO_4$ and solvent was evaporated under reduced pressure. Using column chromatography (1:1, chloroform:hexane), 4,7- dibromo-2-dodecylbenzotriazole was obtained as a light yellow oil (4.3 g, 75 %). ^{1}H NMR (400MHz, CDCl3, δ): 7.36 (s, 2H), 4.60 (t, J=7.0 Hz, 2H), 2.10 (m, 2H), 1.38-1.12 (m, 18H), 0.80 (t, J=6.9 Hz, 3H). ^{1}3CNMR (100 MHz, CDCl3, δ): 143.7, 129.4, 109.9, 57.4, 31.8, 30.1, 29.5, 29.5, 29.4, 29.4, 29.3, 28.9, 26.4, 22.6, 14.0.

2.3.4 Synthesis of Tributyl(thiophen-2-yl)stannane and Tributyl(4-hexylthiophen-2 yl)stannane

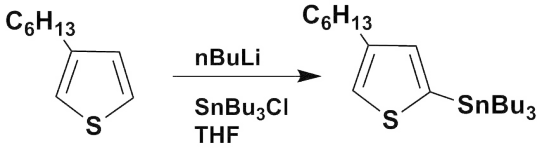

Figure 2.4: Synthetic route for stannylation of thiophene and 3-hexyl thiophene

In the stannylation of thiophene and 3-hexyl thiophene, the same procedure was conducted. A solution of 3-hexyl thiophene (2 g, 2.13 mL) was dissolved in THF (20

mL), and cooled to -78 °C. n-Butyllithium (5.2 mL of 2.5 M) was added drop-wise. At the end of the addition the reaction was warmed to room temperature and stirred for one hour. Then the mixture was again cooled to -78 °C and , tributyltin chloride (3.5 mL) was added at that temperature via a syringe. After addition was completed, reaction was allowed to stir at -78 °C for 4 hour. The reaction then leaved to stir at room temperature for overnight. At the end of the reaction, water was added to the mixture. The phases were separated and organic layer was extracted with CH_2Cl_2, brine and sodium bi carbonate. The organic layer was dried over $MgSO_4$. After removal of the solvent, the product was obtained as a yellow viscous liquid (70 %).^{1}H NMR (400MHz, CDCl3, δ): 7.69 (1H), 7.17 (1H), 7.00 (1H), 1.58, (6H), 1.30 (6H),1.31 (6H), 0.90 (9H).

2.3.5 Synthesis of 2-Dodecyl-4,7-bis(4-hexylthiophen-2-yl)-2Hbenzo[d][1,2,3]-triazole (HTBT)

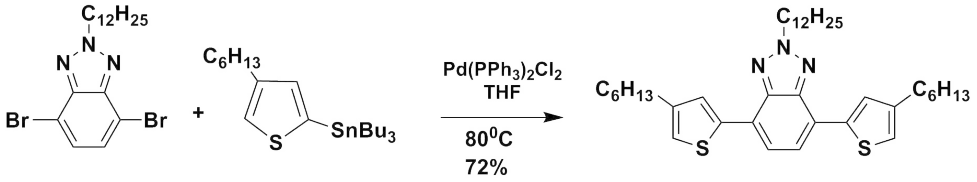

Figure 2.5: Synthetic route for 2-Dodecyl-4,7-bis(4-hexylthiophen-2-yl)-2Hbenzo-[d][1,2,3]triazole (HTBT)

HTBT was synthesized via Stille coupling. To a three-necked round bottom flask were added 4,7-dibromo-2-dodecylbenzotriazole (100 mg, 0.224 mmole), and tributyl(4-hexylthiophen-2-yl)stannane (511 mg, 1.12 mmole). The flask was flushed with argon. 100 ml THF and dichlorobis(triphenylphosphine)-palladium(II) (50 mg, 0.045 mmole) was added at room temperature. The mixture was refluxed for 12 hours under argon atmosphere. After solvent removed, the crude product was purified by column chromatography on silica gel to obtain 95 mg (72 %) HTBT. ^{1}H NMR (400MHz, $CDCl_3$): 7.9 (s, 2H), 7.5 (s, 2H), 6.9 (s,2H), 4.8 (t, J=7.0 Hz, 2H), 2.1 (m, 2H), 1.4-1.1 (m, 18H), 0.9 (t, J=6.9 Hz, 3H); 13C NMR (100 MHz, $CDCl_3$,): 143.1, 140.1, 138.3, 127.1, 122.4, 121.3, 119.0, 55.5, 30.6, 30.5, 29.5, 29.2, 28.8, 28.4, 28.2, 27.8, 25.49, 21.4, 12.8 MS (m/z): 619 [M+].

2.3.6 Synthesis of 4,7-Bis(5-bromo-4-hexylthien-2-yl)-2-dodecylbenzo[1,2,3]triazole

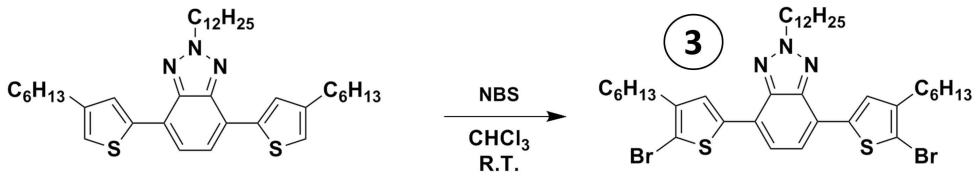

Figure 2.6: Synthetic route for 4,7-Bis(5-bromo-4-hexylthien-2-yl)-2-dodecylbenzo-[1,2,3]triazole

200 mg of 4,7-Bis (3-hexylthien-5-yl) 2-dodecyl-benzo[1,2,3]triazole (0.32 mmole) and 138 mg of N-bromosuccinimide (0.77 mmole) were stirred in 100 ml of $CHCl_3$ at room temperature by preventing the mixture from light exposure. After 12 h solvent was removed under reduced pressure and crude product was filtered over silica by $CHCl_3$ to obtain used to obtain 235 mg (94 %) as yellow solid. ^{1}H NMR (400MHz, $CDCl_3$, δ): 7.72 (d, J=5.6 Hz, 2H), 7.44 (s, 2H), 7.04 (d, J=6.0 Hz, 2H), 4.72 (t, J=7.0 Hz, 2H), 2.10 (m, 2H), 1.32-1.17 (m,18H), 0.80 (t, J=6.9 Hz, 3H); ^{1}3C NMR (100 MHz, $CDCl_3$-d6, δ): 144.4, 142.2, 140.4, 127.3, 125.8, 123.9, 123.0, 57.1, 32.2, 30.3, 29.9, 29.8, 29.7, 29.6, 29.5, 29.3, 26.9, 22.9, 14.4. MS (m/z): 608 [M+].

2.4 Synthesis of the Polymers

Polymers were synthesized by poly condensation Suzuki cross coupling reactions. The synthetic pathway is shown in Figure 2.7.

2.4.1 Synthesis of Poly 4-(biphenyl-4-yl)-4'-tert butylspiro[benzo[d]imidazole-2,1'-cyclohexane] (P1)

4,7-Dibromo-4-(tert-butyl)spiro[benzo[d]imidazole-2,1cyclohexane] (1 mole equivalent), 4,4'-biphenyldiboronic acid bis(neopentyl) ester (1 mole equivalent), $Pd(PPh_3)_4$ (5 mole %) and tetrabutylammonium iodide ($N(Bu)_4I$, 1 mole %) was added into a degassed mixture of potassium carbonate (K_2CO_3, 2M in H_2O), toluene (3:2 toluene :water). The mixture was refluxed for 48 h under argon at 90 °C. Then excess of

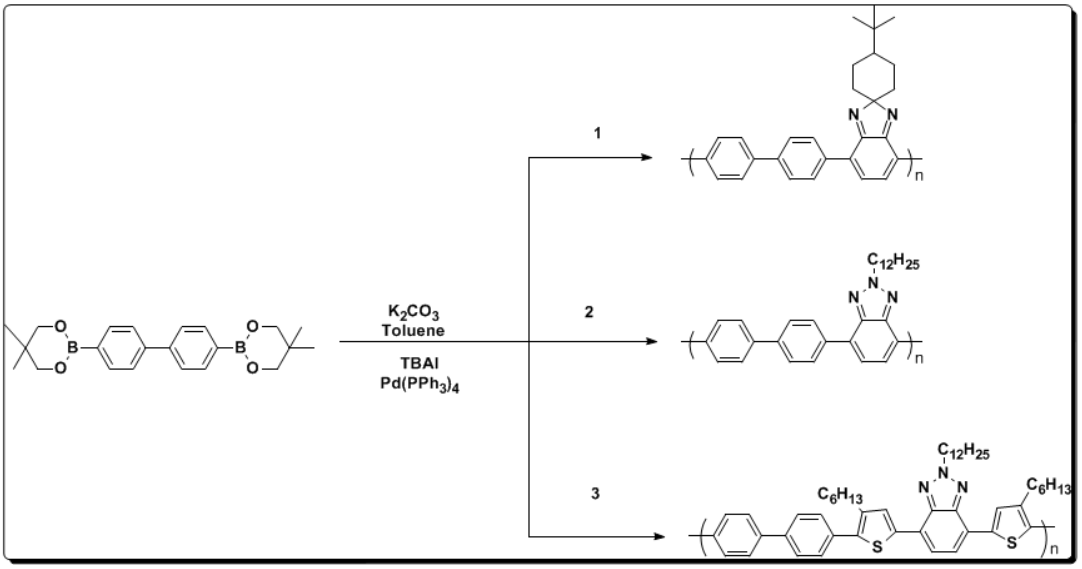

Figure 2.7: Synthetic route for polymers

biphenyldiboronic acid bis(neopentyl) was added as an end capper and the solution was refluxed again for 8 h. After that bromobenzene was added and the solution was further refluxed for another 8 h. After ending the reaction, the solvent was removed and crude mixture was extracted with $CHCl_3$:H_2O. Combined organic layers were dried over anhydrous $MgSO_4$ and evaporated under reduced pressure. The product was purified with methanol, hexane and acetone consecutively to obtain corresponding polymer.

2.4.2 Synthesis of Poly 4-(biphenyl-4-yl)-2-dodecyl-2H-benzo[d][1,2,3]triazole (P2)

4,7-Dibromo-2-dodecylbenzotriazole (1 mole equivalent), 4,4'-biphenyldiboronic acid bis(neopentyl) ester (1 mole equivalent), $Pd(PPh_3)_4$ (5 mole %) and tetrabutylammonium iodide ($N(Bu)_4I$, 1 mole %) was added into a degassed mixture of potassium carbonate (K_2CO_3, 2 M in H_2O), toluene (3:2 toluene :water). The mixture was refluxed for 48 h under argon at 90 °C. Then excess of biphenyldiboronic acid bis(neopentyl) was added as an end capper and the solution was refluxed again for 8 h. After that bromobenzene was added and the solution was further refluxed for another 8 h. At the end, the solvent was removed and crude mixture was extracted with $CHCl_3$:H_2O.

Combined organic layers were dried over anhydrous $MgSO_4$ and evaporated under reduced pressure. The product was purified with methanol, hexane and acetone consecutively to obtain corresponding polymer.

2.4.3 Synthesis of Poly(4-(5-(biphenyl-4-yl)-4-hexylthiophen-2-yl)-2-dodecyl-7-(4-hexylthiophen-2-yl)-2H-benzo[d][1,2,3]triazole (P3)

4,7-Bis(5-bromo-4-hexylthien-2-yl)-2-dodecylbenzo[1,2,3]triazole (1 mole equivalent) 4,4'-biphenyldiboronic acid bis(neopentyl) ester (1 mole equivalent), $Pd(PPh_3)_4$ (5 mole %) and tetrabutylammonium iodide ($N(Bu)_4I$, 1 mole %) was added into a degassed mixture of potassium carbonate (K_2CO_3, 2 M in H_2O), toluene (3:2 toluene :water). The mixture was refluxed for 48 h under argon at 90 °C. Then excess of Biphenyldiboronic acid bis(neopentyl) was added as end capper and the solution was refluxed again for 8 h. After that bromobenzene was added and the solution was further refluxed for another 8 h. At the end the solvent was removed and crude mixture was extracted with $CHCl_3$:H_2O. Combined organic layers were dried over anhydrous $MgSO_4$ and evaporated under reduced pressure. The product was purified with methanol, hexane and acetone consecutively to obtain corresponding polymer.

2.5 Physical Properties

Gel Permeation Chromatography (GPC) is employed to separate the particles according to their size. The material is solved in organic solvents which acts as the mobile phase. Beads of porous polymeric material is used as the stationary phase. Polymer Laboratories Gel Permeation Chromatography (GPC) 220 of the METU Central Laboratory which is calibrated with universal standard polystrene was used to calculate average molecular weights (M_n and M_w). These properties were determined using 5 mg of polymers dissolved in THF.

Thermal stability of the polymers is crucial in device fabrication applications. Therefore the thermal stability of the polymers were examined with the help of Differential Scanning Calorimetry (DSC) and Thermal Gravimetric Analysis (TGA). In DSC study, changes in polymers with the applied heat is examined. Identified thermal

transition properties are such as the glass transition temperature (T_g), the melting temperature (T_m) and the crystallinity temperature (T_c). Perkin Elmer Differential Scanning Calorimetry was used in DSC studies. The experiments were conducted under nitrogen environment and within an 25-250 °C temperature range with the data taken under 10 °C/min intervals. Physical changes and reactions in polymers under applied heat is examined in Thermal Gravimetric Analysis. Change in mass due to thermal degradation in polymers is tracked by this method. It is possible to locate the decomposition temperature of materials by the help of this data.Perkin Elmer Pyris 1 Thermal Gravimetric Analysis was employed in TGA studies. The experiments were conducted under nitrogen environment within an 25-700 °C temperature range and measurements were done under 10 °C/min intervals.

2.6 Electrochemical Characterization

2.6.1 Cyclic Voltammetry

Cyclic voltammetry (CV) is a kind of electrochemical analysis in which the working electrode potential is swept in time between two set values, namely V1 and V2 (See Figure 2.8). This cycle can be accomplished for several times in an experiment. This technique can be applied for the identification of the redox potentials of electroactive species. The current passing through the working electrode is plotted versus the applied voltage to have the cyclic voltammogram (See Figure 2.9).

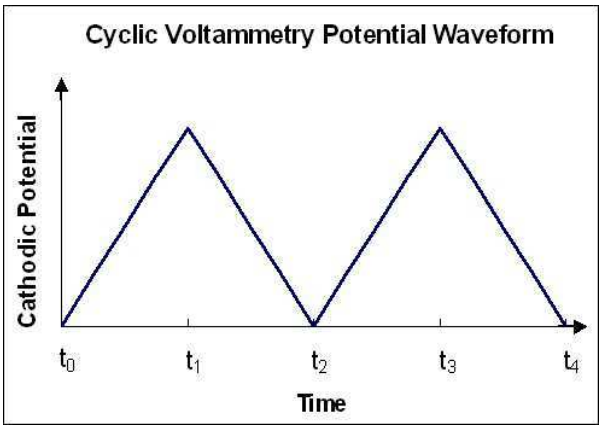

Figure 2.8: Cyclic voltammetry waveform

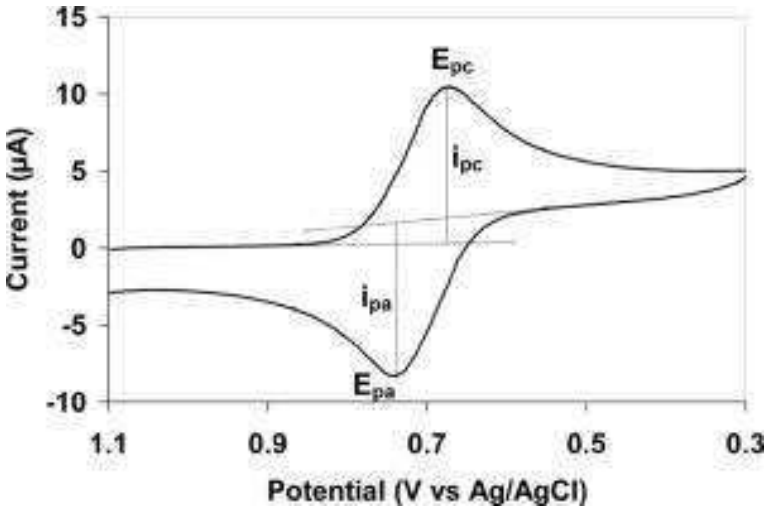

Figure 2.9: A cyclic voltammogram for a reversible redox process

The experimental setup involves three kinds of electrodes which are the working electrode, the reference electrode and the counter electrode. Electrolyte is added to the test solution to provide the required conductivity. The range of the potential is determined by the combination of the solvent, electrolyte and the working electrode.

The counter electrode is made of a material which does not react with the solution. Its purpose is to conduct so that reactions that may occur at the counter electrode surface are unimportant. The counter electrode will often oxidize or reduce the solvent to maintain the observed current.

The applied potential is recorded by a potentiostat during the sweep of the electric potential (which can be seen in Figure 2.8). Estimated response of a reversible redox couple in a single scan can be seen in Figure 2.9. As can be seen from the electrode setup depicted in Figure 2.10 the electric potential is measured between the reference electrode and the counter electrodes and the current is measured from the loop of the working electrode and the counter electrode.

2.6.2 Spectroelectrochemistry

Spectroelectrochemistry is a valuable method which simultaneously combines the techniques of electrochemistry and spectroscopy. A redox active compound is oxi-

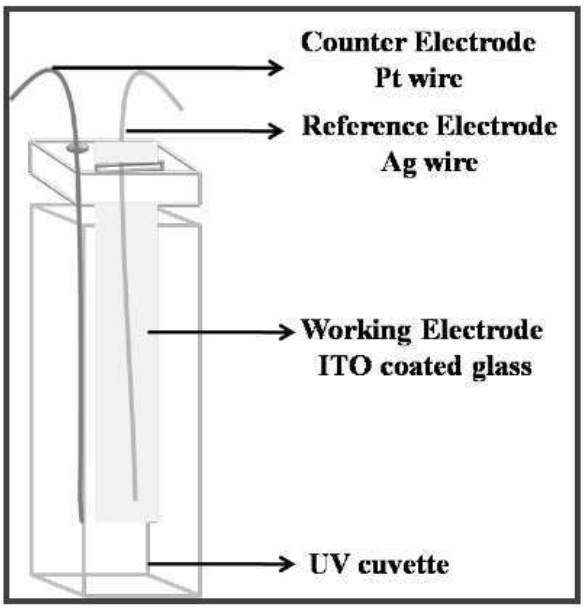

Figure 2.10: Electrode setup

dized or reduced at electrode surface and with the changes in electronic transitions, changes in absorbance are observed. By utilizing this technique, it is possible to provide information about the bang gap, λ_{max}, intergap states (polarons and bipolarons) and colors of the polymer.

Spectral behaviors of each three polymers upon doping were observed by electronic absorption spectra under applied potentials. The polymers were solved in chloroform to a solution of 5 mg/mL and spray coated onto ITO substrate. Then UV-vis-NIR spectra were recorded upon applied potential.

2.6.3 Kinetic Studies

Kinetic studies examine the electrochromic switching time and optical contrast between the neutral and oxidized state. It utilizes square wave potential method coupled with optical spectroscopy which is known as chronoabsorptometry. During the experiment an initial potential is set for a fixed time and then the potential is swept to a second potential and is set for a fixed time again and goes back to the initial value. The absorbance value at a specified wavelength is measured. The specified wavelength is chosen according where the chromophore shows maximum absorbance i.e.

optical contrast by switching potential repeatedly between oxidized and neutral states.

The switching properties of P1, P2 and P3 were studied by spraying them on ITO coated glass slides from chloroform (5 mg/mL) solutions in 0.1 M $TBAPF_6$ in ACN and DCM mixture (9:1) at a scan rate of 50 mV/s. Square-wave potential was performed to respective electrodes between fully oxidized and states.

2.7 Optical Characterization

10 mg/ml solutions of the polymers were prepared and spin coated on glass substrate at 1000 rpm for thin film absorbance and photoluminescence measurements. On the other hand, the solutions were prepared with a concentration of less than 10^{-5} M in order to prevent self-quenching for solution absorbance and photoluminescence measurements. In addition, the cell was degassed with nitrogen to prevent O_2 quenching of the emission during solution photoluminescence measurements.

2.8 OLED Device Application

The OLED structures were fabricated with the configuration of ITO/PEDOT:PSS/-emissive layer/Ca/Al. ITO-coated glasses were purchased commercially which have dimensions as 2.5 cm x 2.5 cm. The specimen was etched and the middle of the specimen was preserved by the utilization of a vinyl tape which masks the middle of the substrater. The non-masked part of the specimen was etched with HCl and zinc dust. After that substrate was put in a 10 % $NaHCO_3$ solution in order to neutralize the acidic area and the slide was washed with water. Finally by immersing the ITO substrates into ultrasonic bath they were washed with toluene, water and detergent, acetone and isopropanol consequently for 15 minutes. The slides were cleaned by O_2 plasma treatment for further purifications.

A thin film of hole transporting material PEDOT:PSS formed on the slides by spin-coating at 5000 rpm and annealed at 150 °C for 15 minutes. After that 10 mg/ml P3-PVK composite films with different weight ratios were spin-coated on them by spin coating at 1000 rpm. The films were put into the vacuum-chamber inside a

nitrogen-filled glove box system (MBraun 200 B with moisture < 0.1 ppm, oxygen < 0.1 ppm) and 20 nm Ca cathode was deposited onto blend films. For preventing the oxidation of the Ca, 80 nm Al layer was deposited as a protecting layer. The shadow-mask is designed such that eight individual device (active layer) with 0.06 cm^2 area are formed.

After electrode deposition, the OLED devices were then encapsulated with glass covers, sealed with UV-cured epoxy glue, in the glove box.

Current-Voltage-Luminance (IVL) and electroluminescence (EL) spectra measurements were conducted outside the glove box with Keithley 2400 source meter and Maya 2000 spectrophotometer from Ocean Optics.

CHAPTER 3

RESULTS AND DISCUSSION

3.1 Synthesis

The polymers were synthesized via Suzuki polycondensation mechanism. P1 was obtained with a yield of 55 %, P2 was obtained with a yield of 67 % and P3 was obtained with a yield of 65 %. P1 has an average-number molecular weight of, Mn, 19700 with poly dispersity index, PDI, 1.58, P2 has Mn of 12200 with PDI of 1.43, P3 has Mn of 8600 with PDI of 3.8, which shows that they have enough number of repeating units for thin film applications.

TGA curves of the polymers shown in appendix show that the polymers had good thermal stability with decomposition of backbone temperatures of (60 % weigth loss from stochiometry) 400 °C, 500 °C and 550 °C respectively (Figure A.1, A.2 and A.3). The highest thermal stability of P3 is due to the lowest repeating unit of the polymer.

The polymers did not possess clear phase transitions in the determination range of DSC which shows that the high glass transition temperatures were up to 250 °C (Figure B.1, B.2 and B.3). As a result they fullfill the requirements of high temperature stability as required for optoelectronic thin-layer devices.

The polymers have good solubility in common organic solvents such as THF, chloroform and DCM. They have good film forming ability cast from solutions.

The chemical structures of the polymers were confirmed with ^{1}H NMR spectroscopy show in Figures 3.1, 3.2 and 3.3 below providing that all the detected peaks are con-

sistent with the proposed structures.

3.1.1 Poly 4-(biphenyl-4-yl)-4'-tert-butylspiro[benzo[d]imidazole-2,1'-cyclohexane]-(P1)

^{1}H NMR (400MHz, $CDCl_3$, δ): 8.4-8.0 (benzimidazole), 7.5-7.0 (biphenyl), 0.9 (tert-butyl), 1.2-1.6 (cyclohexane).

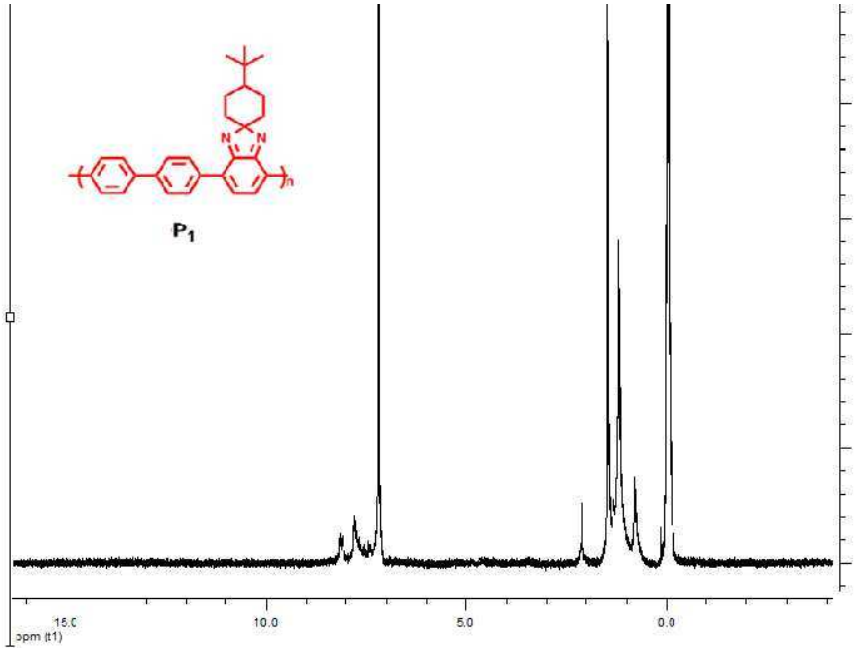

Figure 3.1: ^{1}H NMR of Poly 4-(biphenyl-4-yl)-4'-tert-butylspiro[benzo[d]imidazole-2,1'-cyclohexane] (P1)

3.1.2 Poly 4-(biphenyl-4-yl)-2-dodecyl-2H-benzo[d][1,2,3]triazole (P2)

^{1}H NMR (400MHz, $CDCl_3$, δ): 8.0-7.6 (benzotriazole), 7.5-7.2 (biphenyl-benzotriazole), 3.8 (N-CH_2), 2.5-0.7 (pendant alkyl chains).

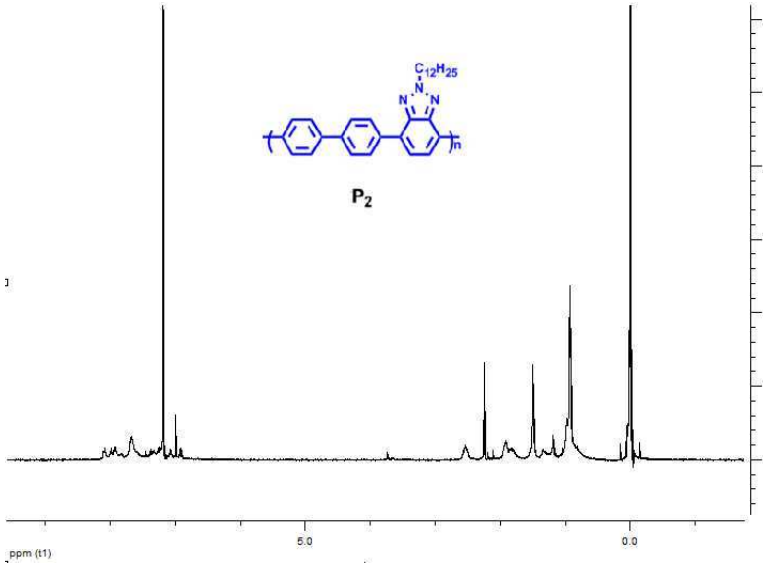

Figure 3.2: ^{1}H NMR of Poly 4-(biphenyl-4-yl)-2-dodecyl-2H-benzo[d][1,2,3]triazole

3.1.3 Poly(4-(5-(biphenyl-4-yl)-4-hexylthiophen-2-yl)-2-dodecyl-7-(4-hexyl-thiophen-2-yl)-2H-benzo[d][1,2,3]triazole (P3)

^{1}H NMR (400MHz, $CDCl_3$, δ): 8.2 (biphenyl), 7.5-7.2 (thiophene, biphenyl), 4.2 (N-CH_2), 2.8 (C-Ch_2), 2.2-0.7 (pendant alkyl chains).

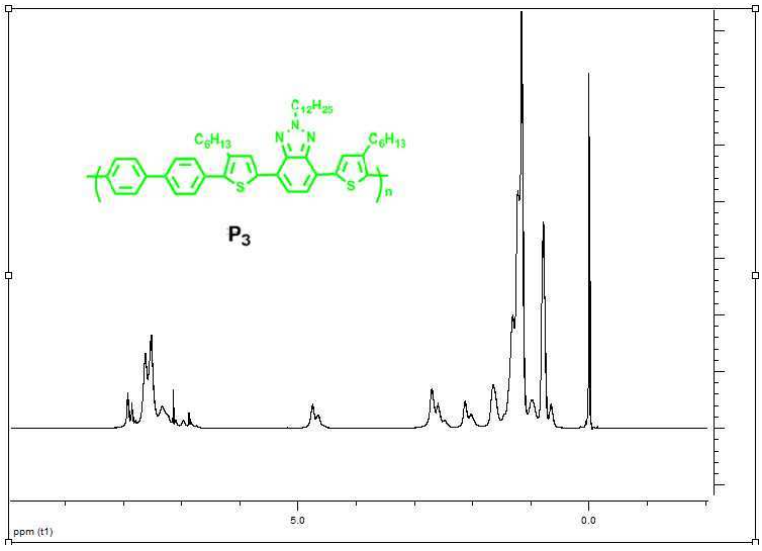

Figure 3.3: Poly(4-(5-(biphenyl-4-yl)-4-hexylthiophen-2-yl)-2-dodecyl-7-(4-hexyl-thiophen-2-yl)-2H-benzo[d][1,2,3]triazole (P3).

3.2 Electrochemical Properties

3.2.1 Cyclic Voltammetry

The electrochemical characterization studies were performed by dissolving polymers in chloroform with a concentration of 5 mg/mL. The dissolved polymers were spray coated onto ITO coated glass specimen.

The polymers were subjected to cyclic voltammetry (CV) analysis to determine the redox potentials under ambient conditions, in 0.1M $TBAPF_6$/ACN solutions at a scan rate 50 mV/s. The specimens were placed in three electrode cells where Pt wire was the counter and Ag wire was the pseudo reference electrode.

The corresponding HOMO/LUMO values were extracted from the cyclic voltammogram. HOMO values were calculated from the oxidation potential onset values and LUMO values were calculated from the reduction potential onset according to Equation 3.1. The value of Normal Hydrogen Electrode (NHE) versus vacuum is -4.75 eV and Fc/Fc^+ versus NHE is 0.3 eV . Corresponding band gaps were calculated from the difference between the HOMO and LUMO values.

$$\begin{aligned} E_{HOMO} &= -(E_{onset,ox} + 4.75 + 0.3)(eV) \\ E_{LUMO} &= -(E_{onset,red} + 4.75 + 0.3)(eV) \\ E^{ec} &= (E_{onset,ox} - E_{onset,red})(eV) \end{aligned} \tag{3.1}$$

For the determination of the redox potentials of P1, the potential was swept between -2.0 V and 1.9 V versus Ag wire pseudo reference electrode. The electrochemical behavior of the polymer is shown in Figure 3.4.

As shown in Figure 3.4 the polymer is p-dopable. P1 film revealed reversible doping/dedoping couple at positive potential pointed as 1.74/1.43 V versus Ag wire pseudo reference electrode. Onset value of oxidation potential is 1.54 V giving HOMO value of 6.59 eV. Irreversible n-doping peak at negative potentials pointed at -1.18 V but detectable n-dedoping potential could not be observed from the voltammogram.

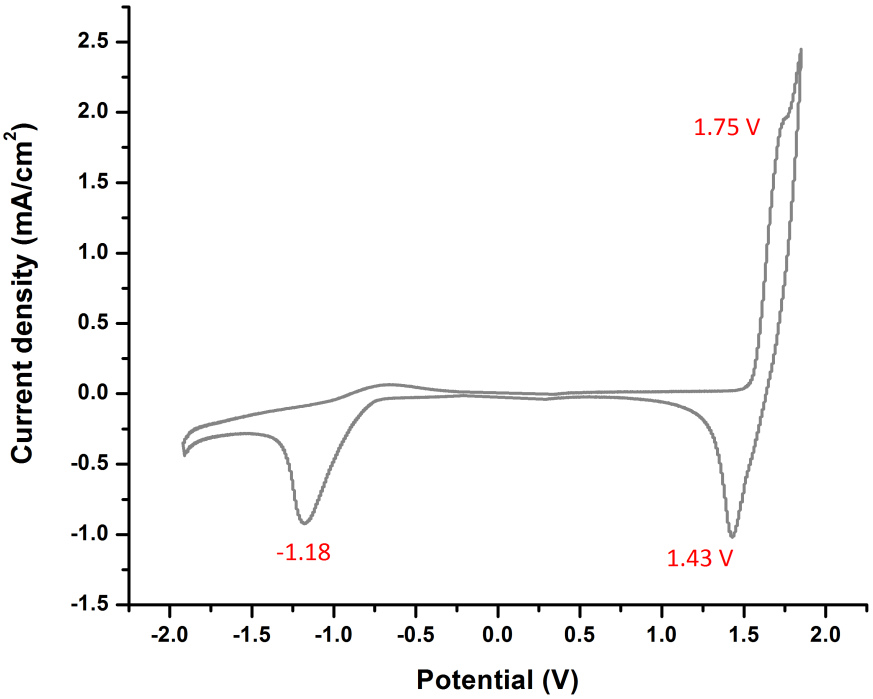

Figure 3.4: Cyclic voltammogram of P1 for both p and n type doping in the presence of 0.1 M $TBAPF_6$/ACN:DCM solution at a scan rate of 50 mV/s

In order to investigate redox potentials of P2, the potential was swept between -2.3 V and 1.9 V. The electrochemical behavior of the polymer is shown in Figure 3.5.

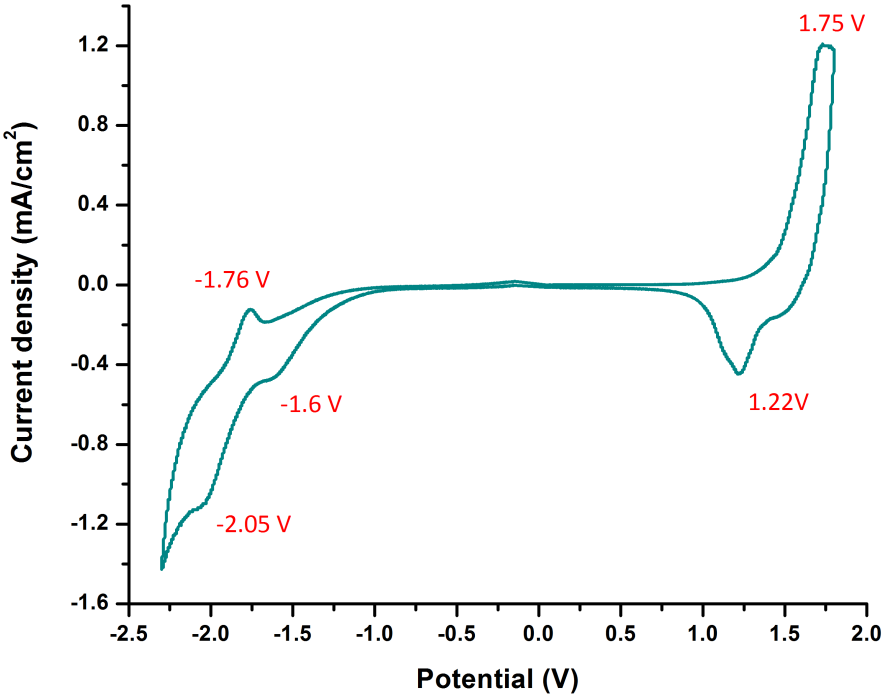

Figure 3.5: Cyclic Voltammogram of P2 for both p and n type doping in the presence of 0.1 M $TBAPF_6$/ACN:DCM solution at a scan rate of 50 mV/s

As depicted in Figure 3.5 the polymer is both p- and n-dopable. P2 film revealed reversible doping/dedoping couple at positive potential pointed as 1.75/1.22 V and reversible n-doping/n-dedoping couple at negative potentials pointed at -1.60 & -2.05/-1.76 V versus Ag wire pseudo reference electrode. Onset value of oxidation potential is 1.44 V revealing an HOMO value of 6.49 eV. Onset value of reduction potential is -1.16 V giving a LUMO value of 3.89 eV. Electronic bandgap value was calculated as 2.6 eV.

The determination of the redox potentials of P3 was performed by sweeping the potential between -2.4 V and 1.5 V. The electrochemical behavior of the polymer is shown in Figure 3.6.

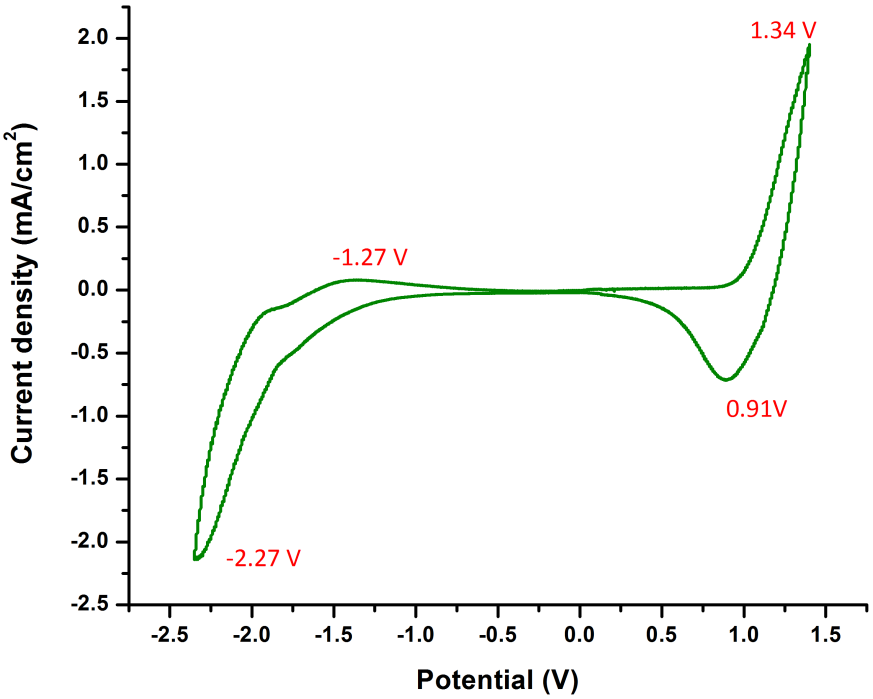

Figure 3.6: Cyclic voltammogram of P3 for both p and n type doping in the presence of 0.1 M $TBAPF_6$/ACN:DCM solution at a scan rate of 50 mV/s

P3 film revealed reversible doping/dedoping couple at positive potential pointed as 1.34/0.91 V and reversible n-doping/n-dedoping couple at negative potentials pointed at -2.27/- 1.27 V versus Ag wire pseudo reference electrode. Onset value of oxidation potential is 0.98 V showing an HOMO value of 6.03 eV. Onset value of reduction potential is -1.58 V giving a LUMO value of 3.47 eV. Electronic bandgap value is calculated as 2.56 eV.

The investigation of n- and p-type doping properties of the polymers enabled the determination of HOMO and LUMO values of polymers from the oxidation and reduction onset values calculated from the intersection of the base line and the line which is tangent to the increasing part of the current due to the ambipolar characteristics of them. Table 3.1 summarizes the onset redox potentials, HOMO-LUMO energies and band gap values for polymers P1, P2 and P3.

Table 3.1: Electrochemical properties of P1, P2 and P3

	Oxidation Potential (V)		Reduction Potential (V)		Band Gap (eV)		Energy Levels	
	E_{ox}	E_{ox}^{onset}	E_{red}	E_{red}^{onset}	E_g^{ec}	$E_g^{op\ a}$	HOMO	LUMO
P1	1.75	1.54	1.43	-0.81		2.14	6.59	4.45[b]
P2	1.75	1.44	1.22	-1.16	2.6	2.35	6.49	3.89
P3	1.34	0.98	0.91	-1.58	2.56	2.33	6.03	3.47

[a]: LUMO value is calculated by using the optical bandgap
[b]: LUMO value is calculated by using the optical bandgap

Relatively electron poor moiety phenyl in P2 makes the electron extraction more difficult than its thiophene counterpart (The oxidation potential, E_{ox} of the TBT counterpart is provided by Balan et al as 1.2 V [48]). Introduction of electron rich hexyl thiophene unit into the backbone in the case of P3 however makes the electron extraction (oxidation) easier and increases the HOMO value.

Changing the acceptor unit in the case of P1 compared to P2 did not change the oxidation potential because they have same electron donor units. In contrast decrease in reduction potential should have been observed because of the fact that the carbon atom in the BIm moiety does not have lone pairs like nitrogen in the BzT moiety which make the group more electron deficient and thus strong acceptor. However, this was not the case since three dimensional network structure of spirocyclohexane

prevents the ion entrance and makes the reduction more difficult.

3.2.2 Spectroelectrochemistry

Spectral behaviors of each three polymers upon doping were observed by electronic absorption spectra under applied potentials. The polymers were dissolved in chloroform to a solution of 5 mg/mL and spray coated onto ITO substrate. Then UV-vis-NIR spectra were recorded upon applied potential for the corresponding polymer film in 0.1 M $TBAPF_6$/ACN solution.

Absorbance changes of P1 were recorded while the potential was swept from 0 to 1.275 V. Spectroelectrochemical properties of P1 is shown in Figure 3.7.

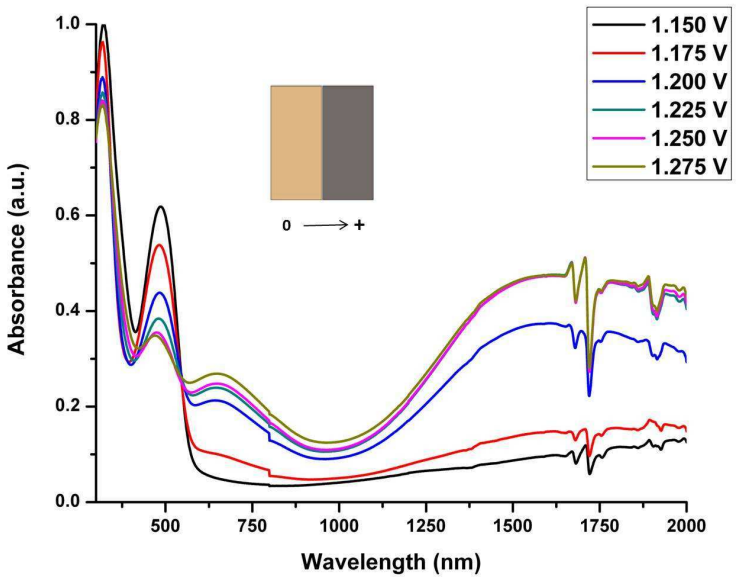

Figure 3.7: p-Doping electronic absorption spectrum of P1 between 0.0 V and 1.275 V in 0.1 M $TBAPF_6$/ACN:DCM electrolyte-solvent couple (0: neutral state, +: oxidized state)

P1 revealed orange color with a λ_{max} value of 481 nm at the neutral state. The absorption onset at 580 nm gave an electronic bandgap of 2.14 eV. As the potential was increased, the absorptions in the visible region started to decrease initiating polaron and bipolaron band formation. The λ_{max} value of intergap states were located as 653 and 1573 nm reached at 1.275 V. The corresponding color revealed as blue.

Absorbance changes of P2 were recorded while the potential was swept from 0 to 1.6 V for p-doped spectrum in Figure 3.8.

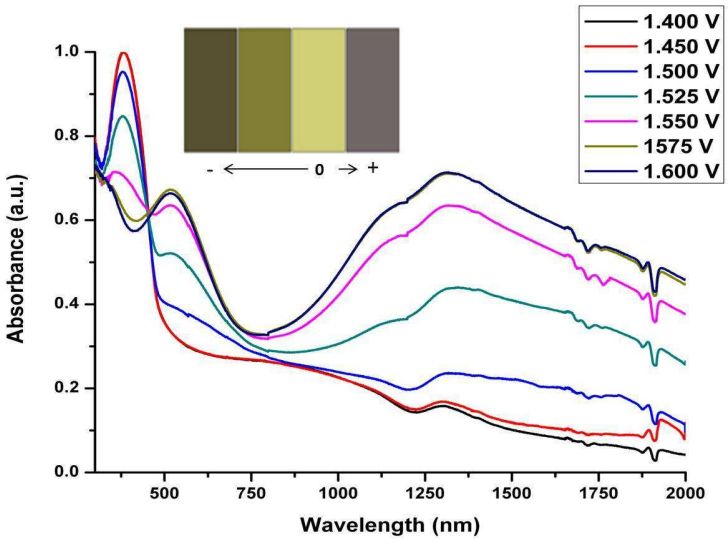

Figure 3.8: p-Doping electronic absorption spectrum of P2 between 0.0 V and 1.275 V in 0.1 M $TBAPF_6$/ACN:DCM electrolyte-solvent couple (0: neutral state, +: oxidized state, -: reduced states)

P2 exhibited yellow color with a λ_{max} value of 387 nm at the neutral state. The electronic bandgap is found as 2.35 eV from the absorption onset at 564 nm. The absorptions in the visible region started to decrease as the potential was increased, which started polaron and bipolaron band formation. The λ_{max} value of intergap states were revealed as 559 and 1320 nm reached at 1.6 V which is the characteristic of violet.

Absorbance changes of P3 were recorded while the potential was swept from 0 to 1.26 V for p-doped spectrum in Figure 3.9. P3 displayed yellow-orange color with a λ_{max} value of 431 nm at the neutral state. The absorption onset at 532 nm gave an electronic bandgap of 2.33 eV. As the potential was increased, the absorptions in the visible region started to decrease initiating polaron and bipolaron band formation. The λ_{max} value of intergap states were located as 697 and 1313 nm reached at 1.26 V. The corresponding color revealed as blue.

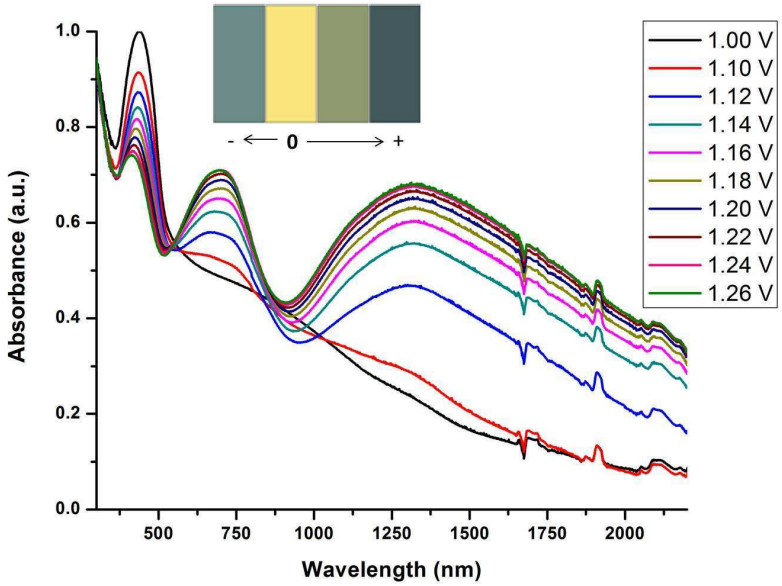

Figure 3.9: p-Doping electronic absorption spectrum of P3 between 0.0 V and 1.275 V in 0.1 M $TBAPF_6$/ACN:DCM electrolyte-solvent couple (0: neutral state, +: oxidized states, -: reduced state)

3.2.3 Kinetic Studies

The polymers films were subjected to successive potential cycling in monomer-free solutions to examine the electrochemical stability and the percent transmittance changes. In order to observe the changes between neutral and fully oxidized states of polymers, kinetic studies were conducted in ACN/$TBAPF_6$ solution. Percent transmittance changes were continuously monitored at dominant wavelengths during switching between 0.0 V and 1.2 V in 0.1 M $TBAPF_6$/ ACN solution for 5 s time intervals by means of a UV-vis-NIR spectrophotometer. Consecutive switching studies of P2 and P3 are shown below in Figure 3.10 and 3.11.

From Figure 3.10, it can be seen that P2 exhibits 10 % optical contrast with a switching time of 1.8 s in the visible region. In the NIR region it revealed 32.33 % optical contrast with a switching time of 4.07 s.

From Figure 3.11, it can be seen that P3 exhibits 24.5 % optical contrast with 3.3 s switching property in visible region. In the NIR region 29.4 % optical contrast with 4.7 s switching time was observed. P3 has extra alkyl chains on the backbone

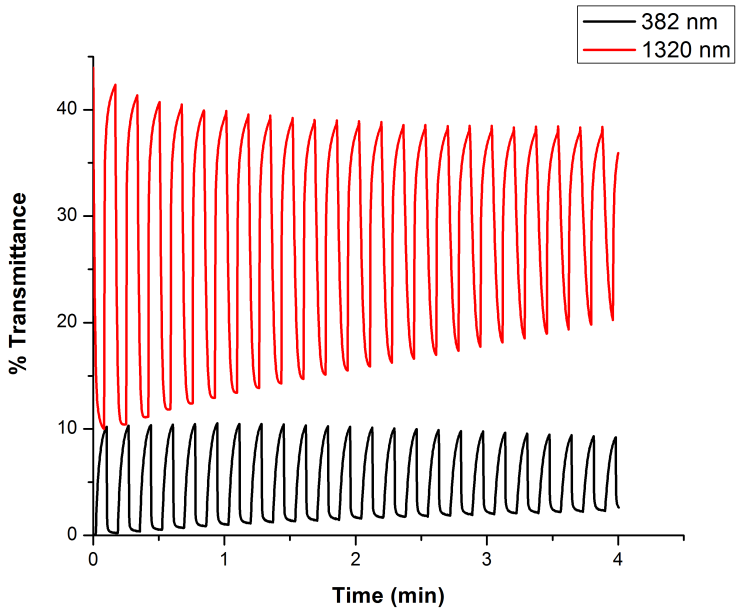

Figure 3.10: Kinetic switching studies of P2

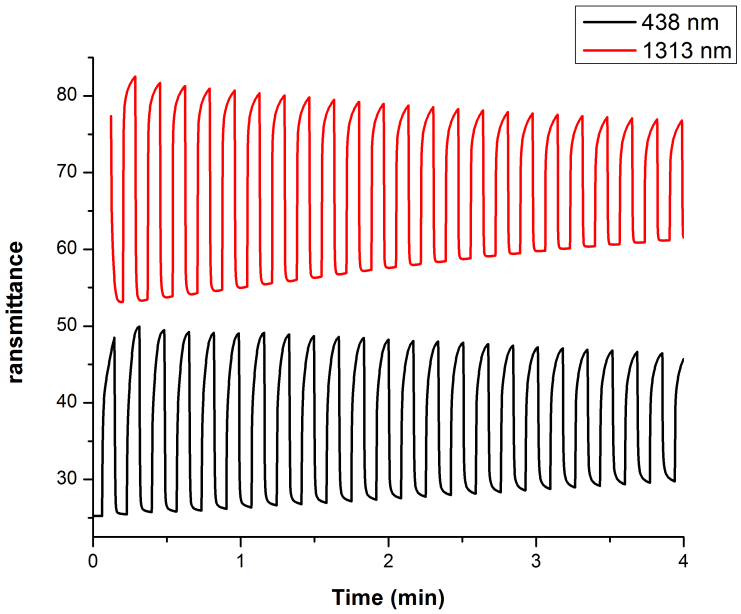

Figure 3.11: Kinetic switching studies of P3

comparing to P1, which makes the ion diffusion more difficult. In addition to this, extended rigidity makes the switching ability weaker. All transmittance measurements are summarized in Table 3.2.

Kinetic studies for P1 revealed switching time more than 5 s which shows that it is not applicable for electrochromic applications.

Table 3.2: Kinetic properties of P2 and P3

	VISIBLE			NIR		
	λ_{max}	ΔT %	Swit. T.	λ_{max}	ΔT %	Swit. T.
P2	1320	10	1.8	382	32.33	4.07
P3	1313	24.5	3.3	438	29.4	4.7

3.3 Optical Properties

The samples were prepared as explained in the Section 2.7. The spectral behaviors are discussed below.

Absorbance spectra of P1, P2 and P3 in thin film and solution are shown in Figure 3.12.

P1 shows λ_{max} absorption value of 467 nm in solution and 481 nm in thin film which is 14 nm red shifted. The carbon moiety in the imidazole unit does not have lone pairs like nitrogen moiety in triazole unit. This electron deficiency of P1 compared to P2 stabilizes LUMO energy level results in longer wavelength absorption. Moreover increase in backbone planarity with spiro units also contributes to the extended conjugation [49].

P2 reveals λ_{max} absorption value of 381 nm in solution and 387 nm in thin film which is 6 nm red shifted.

P3 exhibits λ_{max} absorption value of 423 nm in solution and 431 nm in thin film which is 8 nm red shifted. Extended conjugation with the thiophene unit makes the polymer absorbance at longer wavelength compared to P2.

Emission spectra of P1, P2 and P3 in thin film and solution are depicted in Figure 3.13

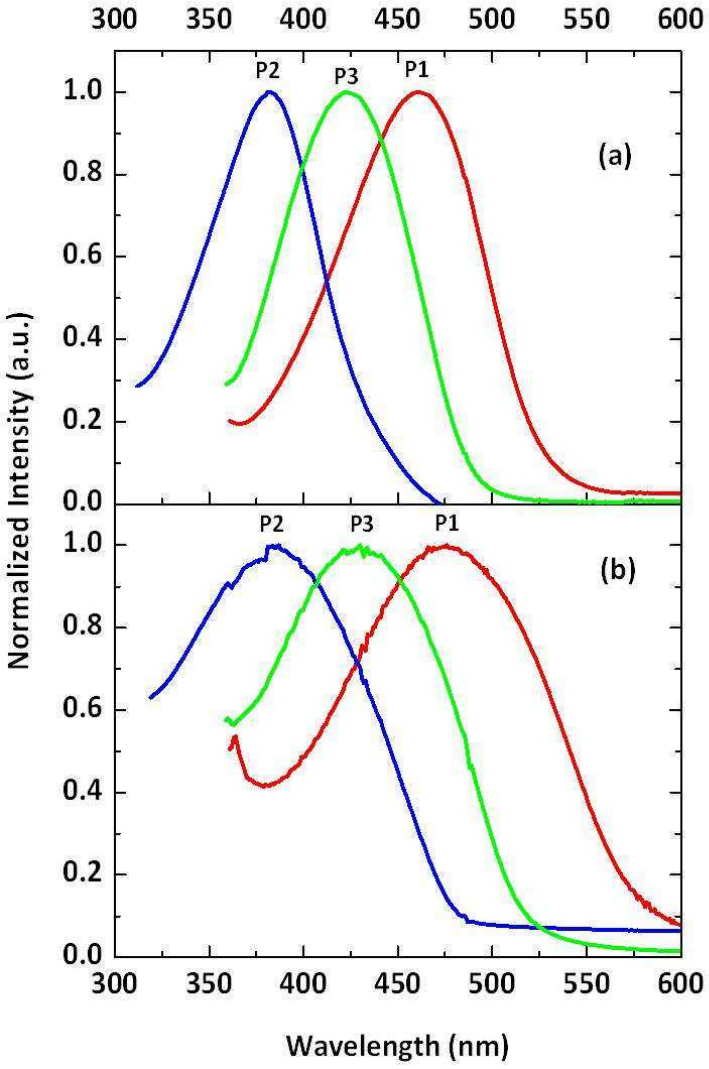

Figure 3.12: Normalized absorption spectra of P1, P2 and P3 (a): Solution, (b): Thin film

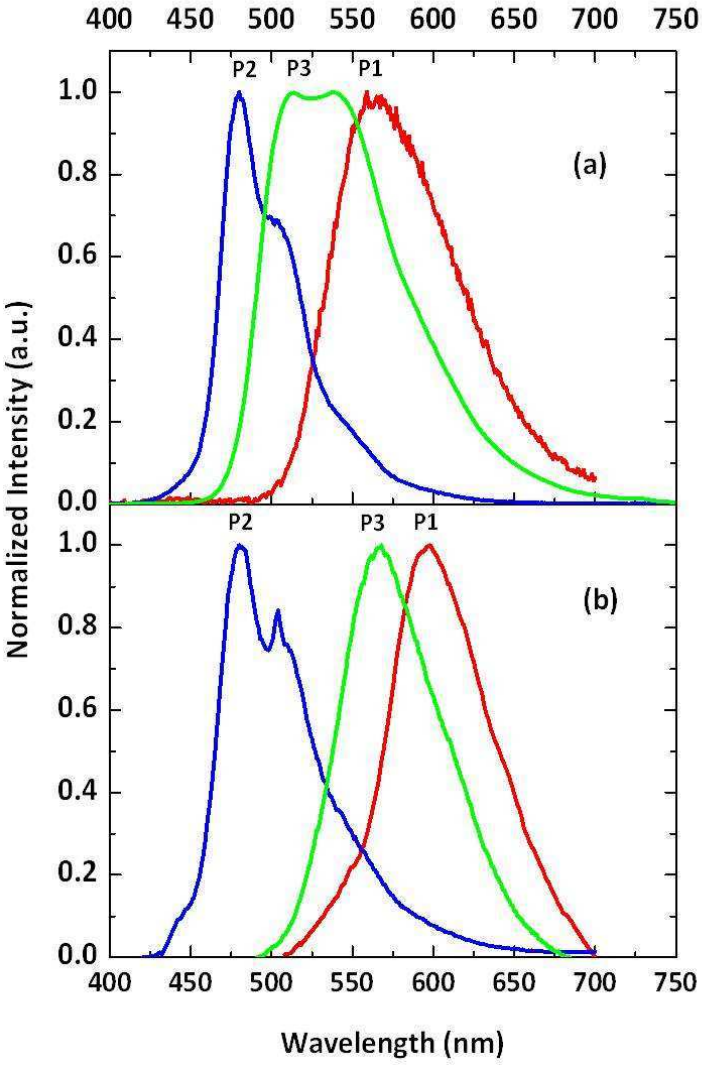

Figure 3.13: Normalized emission spectra of P1, P2 and P3 (a): Solution, (b): Thin film

All the polymers are excited with a wavelength of 420 nm. P1 emits light with λ_{max} values of 564 nm in solution and 599 nm in thin film which is 35 nm red shifted. The emission color for thin film is orange. Whereas, P2 reveals the dominant emission wavelength which possesses 0-0 transition occurring at 481 nm with a well-defined 0-1 transition at 503 nm in solution. The thin film spectrum is broadened but slightly red shifted providing λ_{max} value at 482 nm with a shoulder of 504 nm.The dominant emission color in thin film is blue. P3 displays emission centered at 509 nm in solution. The λ_{max} value for thin film is 567 nm showing yellowish green color and 58 nm red shift is observed.

For photoluminescence efficiency measurement, quinine sulfate reference was used whose emission and absorption spectra in solution are shown in Figure 3.14 below. Its efficiency is 0.55 in H_2SO_4 [50].

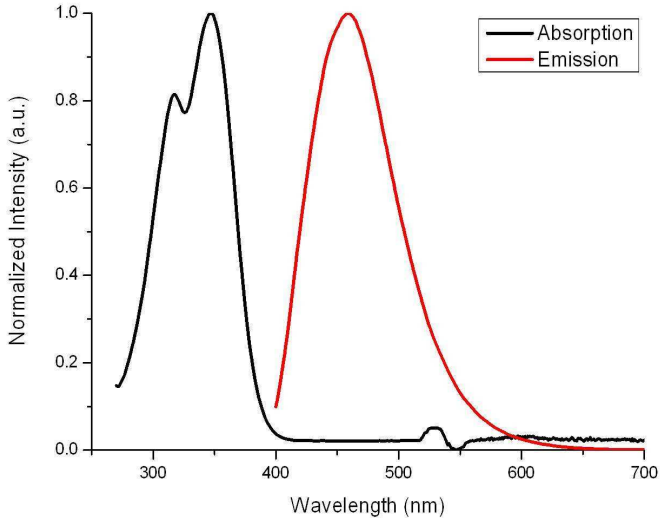

Figure 3.14: Normalized absorption and emission spectra of QS in solution

P2 and P3 display similar absorption and emission behavior as quinnine sulphate which is suitable for quantum efficiency calculations. The calculations were established according to Equation 3.2.

$$\phi_s = \frac{A_s n_r \int F_r}{A_r n_s \int F_s} \phi_r \tag{3.2}$$

In Equation 3.2, ϕ_s and ϕ_r denotes photoluminescence quantum efficiencies, A_s and A_r represents absorbance values at the excitation wavelength, F_s and F_r denotes fluorescence values and n_s and n_r are refractive indices of mediums of sample and reference respectively. Note that the solutions should be very dilute (in the order of 10^{-6} M) providing that maximum absorbance values should not exceed unity to prevent self-quenching.

Calculations reveal 0.701 quantum yield of P2 and 0.57 for P3.

Overall optical properties of P1, P2 and P3 are shown in Table 3.3.

Table 3.3: Optical properties of P1, P2 and P3

Sample	λ_{max}^{Abs} (nm)^a	λ_{max}^{Abs} (nm)^b	λ_{max}^{PL} (nm)^a	λ_{max}^{PL} (nm)^b	ϕ_{PL}
P1	467	481	564	599	-
P2	381	387	481, 503	482, 504	0.701
P3	423	431	509	567	0.57

^{a}: solution
^{b}: thin film

In thin films decrease in intermolecular distances results in π-π stacking which yields longer wavelength emission/absorbance [51, 52]. In addition, the occurrence of aggregation and increased inter/intra-molecular interactions cause inter/intra-molecular excimers/exciplexes for the thin film emission [53]. Those excimers/exciplexes decay non-radiatively or radiatively in the longer wavelength region and this results in a broader and more red-shifted emission.

The energy loss of P2 due to photooxidational deformation of the spatial energy levels is lower than P3 (corresponding Stokes shifts are 117 nm and 144 nm in solution respectively). Furthermore its absorption and emission spectral overlap which confirms the reabsorption of the emitted light, is lower than P3. Therefore it has higher photoluminescence quantum efficiency.

3.4 Device performance

The OLEDs were fabricated as explained at the experimental part (see Section 2.8). The IVL curves and electroluminescence spectra are discussed below. Figure 3.15

and 3.16 reveal the IVL characteristics and the corresponding energy levels of the device fabricated of P3 as the emissive layer. The height of the barrier for hole injection is 0.83 eV and 0.57 eV for electron injection. The device performs a maximum luminance of 267 cd/m^2 at 11.5 V. Beyond this voltage the rapid degradation of device occurs. The device reveals a moderate efficiency of 0.05 cd/A at 3.5 V.

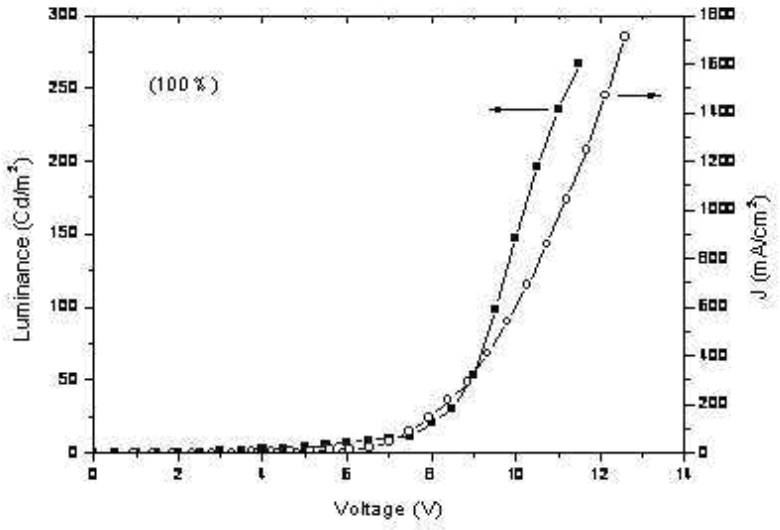

Figure 3.15: IVL characteristic of OLED with P3 emissive layer

Figure 3.17 shows the electroluminescence spectrum of the device together with the photoluminescence spectrum in order to compare the emission processes. The device emits light with a dominant wavelength of 558 nm in a good agreement with its photoluminescence emission at 567 nm. The CIE coordinates are 0.39 and 0.54 (x,y) which are the characteristics of yellow green light. The photoluminescence and electroluminescence spectra are in good agreement providing that dominant emission mechanisms are the same for both processes.

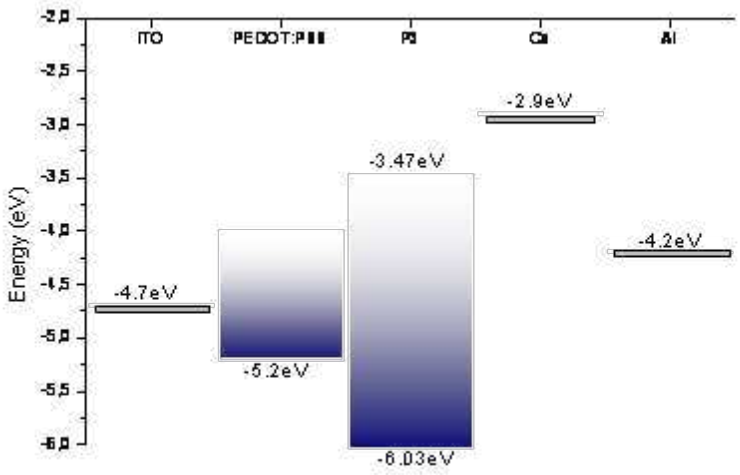

Figure 3.16: Energy levels of the fabricated device

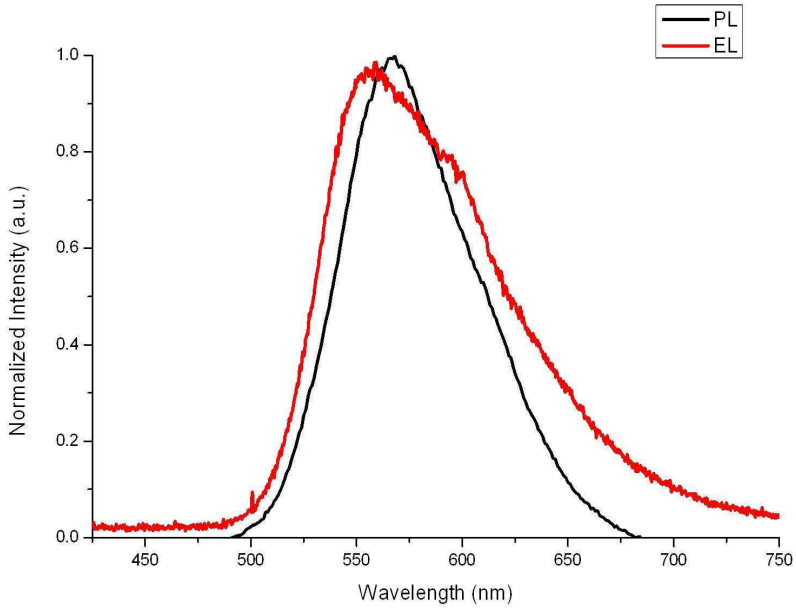

Figure 3.17: Electroluminescence and photoluminescence spectra of P3

3.4.1 Energy Transfer Study

In order to improve device outputs, energy transfer studies were performed. Blue emitting polyvinylcarbazole (PVK) was chosen as the donor material. In Figure 3.18-a the emission spectrum of PVK and absorption spectrum of the P3 show a great overlap that serves one of the basic requirements of the efficient Förster energy transfer conditions. Figure 3.18-b shows the corresponding energy levels of donor and acceptor.

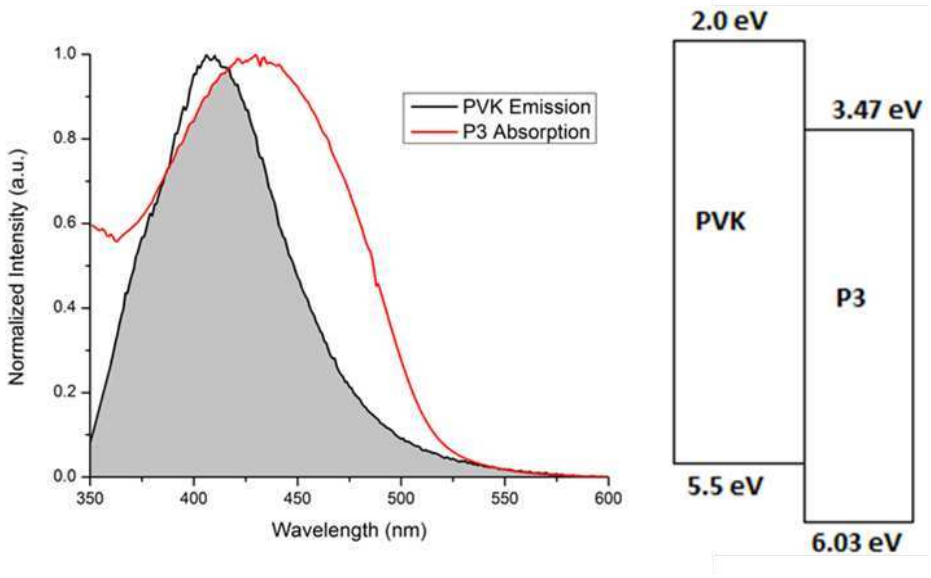

Figure 3.18: Left: Spectral overlap of PVK emission and P3 absorption, Right: energy level diagram of PVK and P3

Single emissive layer blends were prepared with donor to acceptor blend ratios of 95:5, 90:10, 80:20, 70:30, 60:40 with a configuration of ITO/PEDOT:PSS/BLEND/Ca.

Thin film photoluminescence spectra of all blends were taken which is provided in Figure 3.19. As can be seen from the figure, even at very low concentration of the acceptor no emission from the donor (PVK) is observed. This indicates that energy transfer from the donor to the acceptor is successfully achieved.

Electrical and spectral characteristics of OLED devices with all blends are shown in Figure 3.20- 3.24.

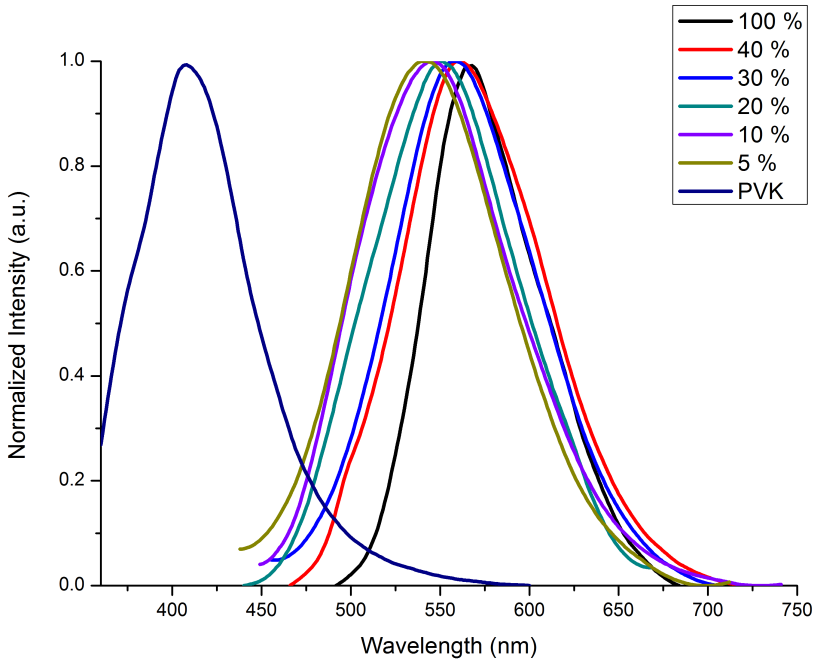

Figure 3.19: Photoluminescence spectrum of all blends as compared with PVK emission

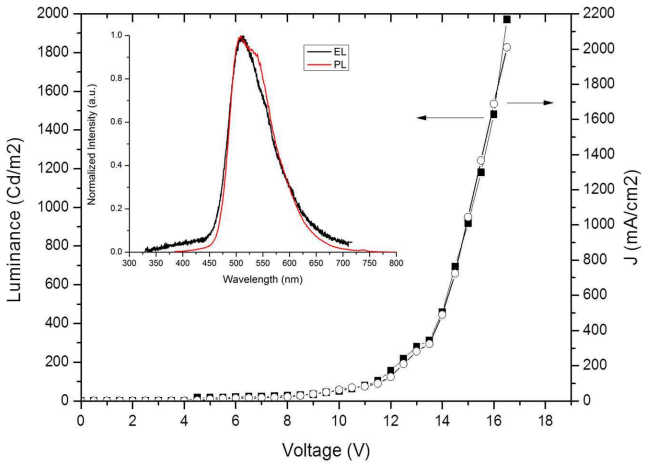

Figure 3.20: Luminance versus voltage and current density of 5 % blend device. The inner caption presents the EL and PL spectra

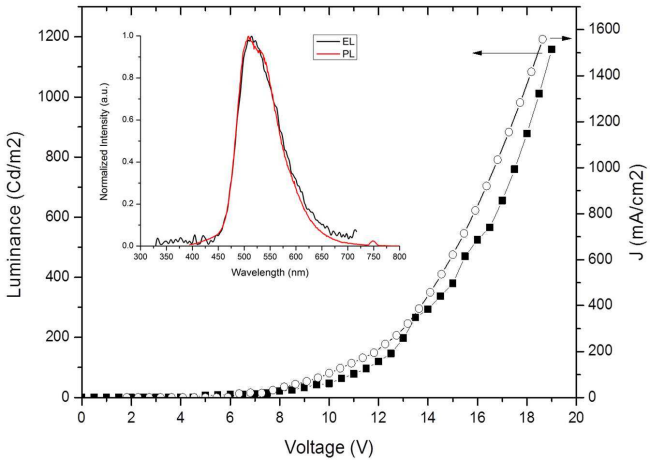

Figure 3.21: Luminance versus voltage and current density of 10 % blend device. The inner caption presents the EL and PL spectra

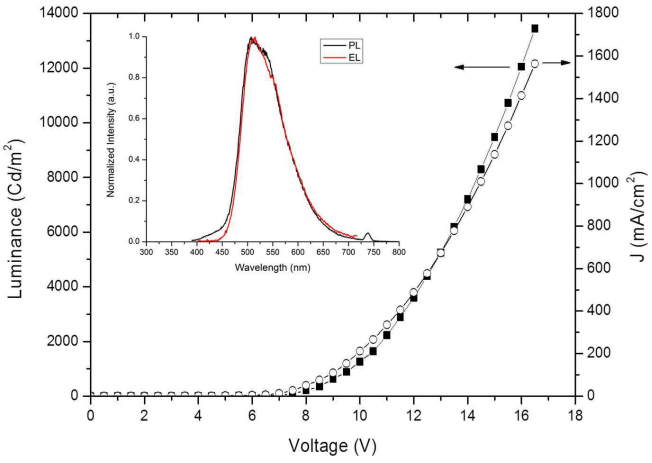

Figure 3.22: Luminance versus voltage and current density of 20 % blend device. The inner caption presents the EL and PL spectra

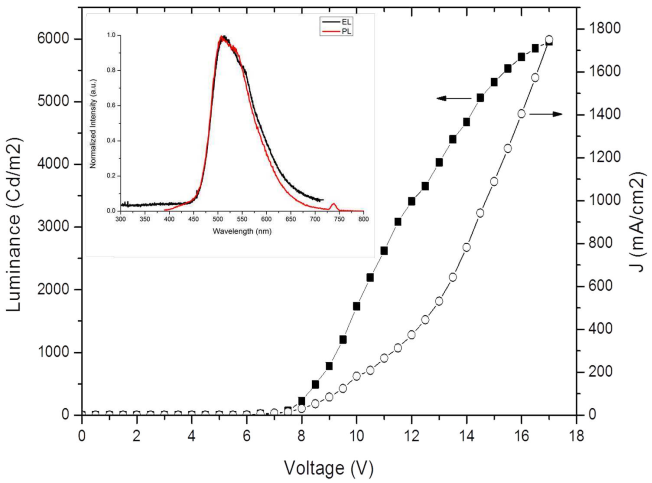

Figure 3.23: Luminance versus voltage and current density of 30 % blend device. The inner caption presents the EL and PL spectra

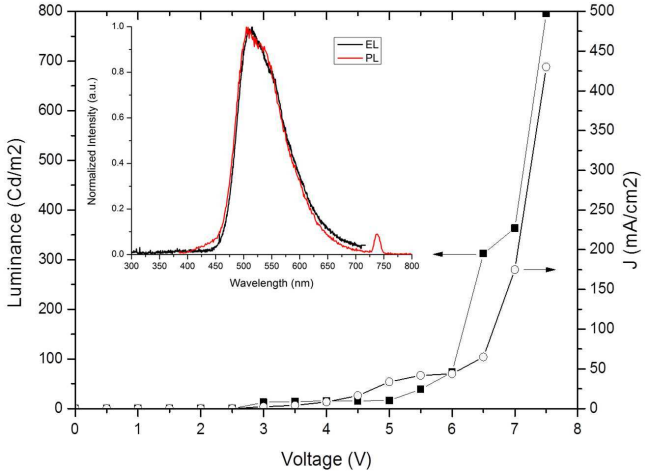

Figure 3.24: Luminance versus voltage and current density of 40 % blend device. The inner caption presents the EL and PL spectra

Regarding the depicted data in Figure 3.20- 3.24; the electroluminescence and solution photoluminescence spectra of all blends are in good agreement. The turn on voltages of all devices are below 3 V. However, if the luminance and current density versus voltage curves are compared, it can clearly be seen that the performances are increased for the blends compared to pure material. For instance, the necessary voltages for the luminance value of 200 cd/m^2 are 11 V for the pure material with the luminance efficiency of 0.023 cd/A, 6 V for the 40 percent blend with the luminance efficiency of 0.3 cd/A, 7.5 V for the 30 percent blend with the luminance efficiency of 0.75 cd/A, 8 V for the 20 percent blend with the luminance efficiency of 0.42 cd/A, 12 V for the 10 percent blend with the luminance efficiency of 0.06 cd/A and 12.5 V for the 5 percent with the luminance efficiency of 0.05 cd/A. The voltages are increased for the 5 and 10 percent blends because of the increase in the average distance of an exciton located on P3 chain segment between PVK segments. Low concentration of the material yields high distance and lower probability of meeting of the charges [54]. Still they reveal better performances compared to the pure material which might be due to the elimination of aggregational quenching.The luminance efficiency of all blends are shown below in Figure 3.25.

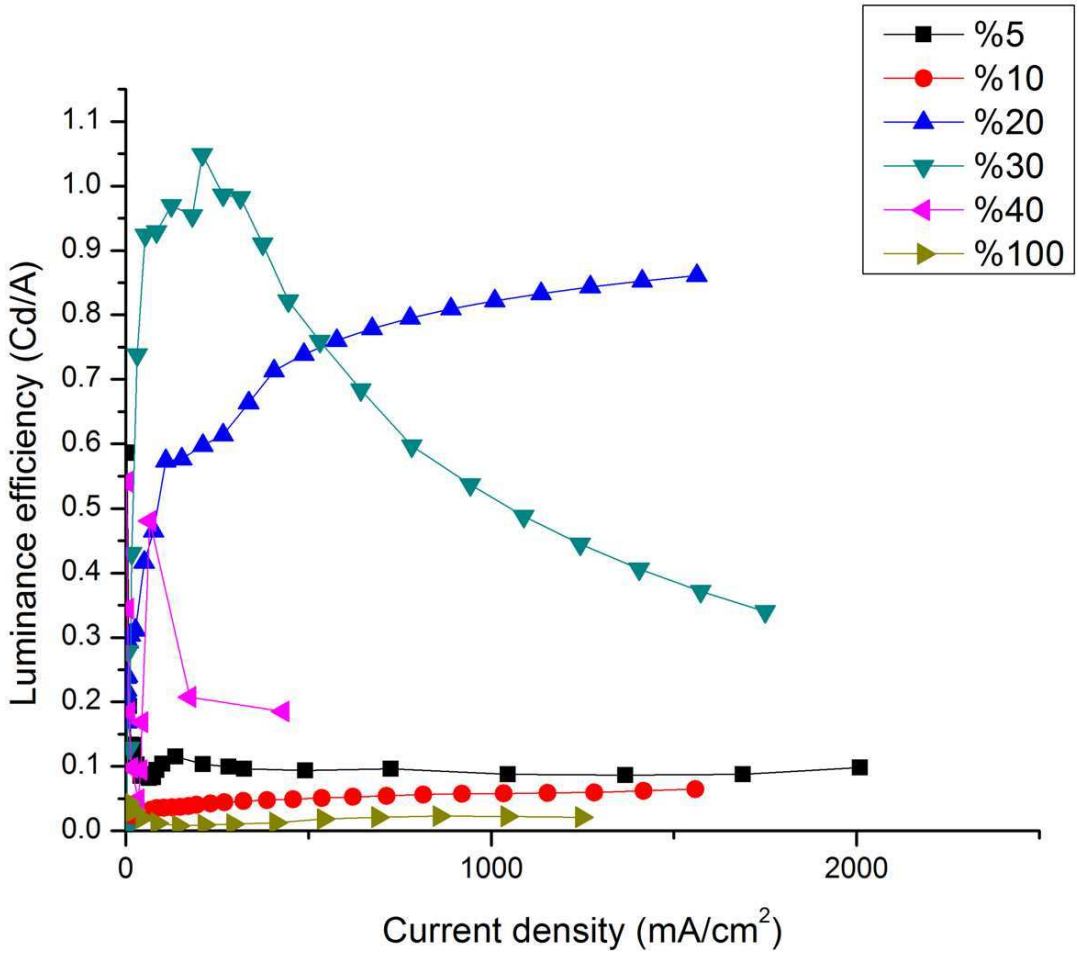

Figure 3.25: The luminance efficiencies of all polymer blends

The color of emission is highly dependent on blend ratio [55]. Isolation of P3 decreases the importance of the green emission due to reduction in intra/inter-chain interaction of pure P3 that leads to more red shifted and lower energy emission. The color chromaticity diagram is shown in Figure 3.26; in which it can be seen that the CIE chromaticity coordinates deviate to the blue emitting region as the percentage of the acceptor is decreased.

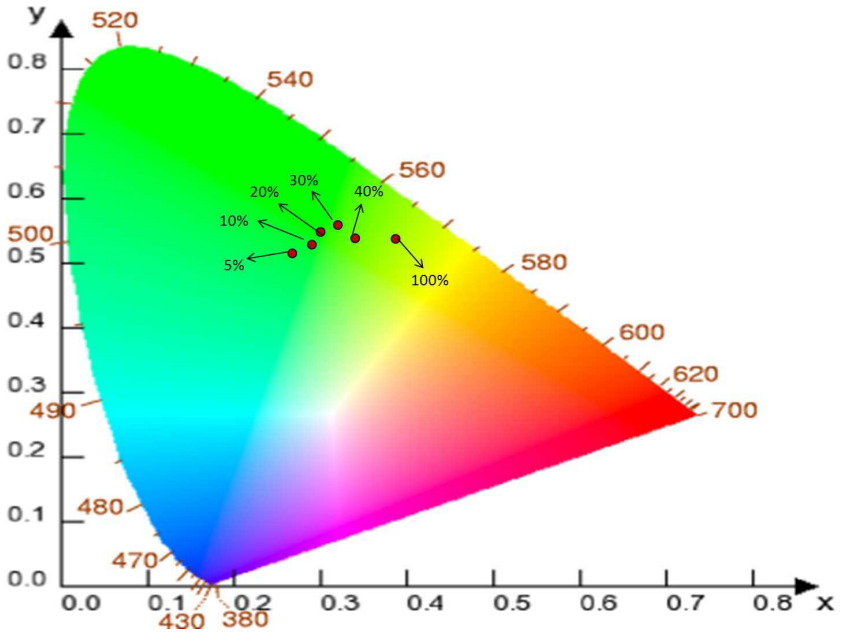

Figure 3.26: The CIE choramaticity diagram of all blends

The change in OLED performances of blends with changing P3 ratio is summarized below in Table 3.4.

Table 3.4: OLED performances as a function of varying P3 ratio

P3 Ratio	λ_{max}^{EL} (nm)	λ_{max}^{PL}* (nm)	Maximum Luminance (cd/m^2)	Luminance Efficiency (cd/A)	CIE Coordinate (x,y)
5 %	508.2	541	1971 (16.5 V)	0.6 (4.5 V)	0.27, 0.52
10 %	510.4	545	1158 (19 V)	0.07 (18.5 V)	0.29, 0.53
20 %	510.6	550	13453 (16.5 V)	0.9 (16.5 V)	0.30, 0.55
30 %	511.6	558	2398 (12 V)	1.1 (10.5 V)	0.32, 0.56
40 %	513.4	560	796 (7.5 V)	0.55 (3 V)	0.34, 0.54
100%	558	567	267 (11.5 V)	0.05 (3.5 V)	0.39, 0.54

*: Thin film

From Table 3.4, it can be perceived that the emission wavelength remains similar for all ratios and no emission from PVK is observed even if at very low concentrations. The maximum luminance values are increased by the applied process and the luminance efficiency of each blend which is an indication of electron to photon power conversion is increased for each blend with respect to pure P3. As an example, for 30 % blend, 1.1 cd/A value is reached for maximum luminance efficiency. This states that the energy transfer is successfully performed.

Förster energy transfer is related to the interaction distance of donor and acceptor as well as it depends on the spectral overlap [56]. As a result, more efficient energy transfer must be achieved as the acceptor concentration is increased. However, aggregation and intermolecular chain interactions are increased as the concentration is increased resulting in non-radiative excimer relaxation [54]. Therefore, the effects of these two phenomena compete. It can be seen from the values given in Table 4.4, the optimum concentration is achieved in 30 % blend ratio which possesses 1.1 cd/A luminance efficiency. This is followed by 20 % blend ratio with a 0.9 cd/A luminance efficiency. Thus it is evaluated that the lower performance of low acceptor percentage blends with respect to 20 and 30 % can be can be attributed to the higher interaction distance. In contrast, the low performance of higher acceptor percentage blend (40 %) can be attributed to the aggregation states probably even in phase separation which results in emission quenching and increased interaction distance.

The PL spectra of the blends' thin films shifted to the red region when compared to their EL spectra. The reason of the difference between EL and PL spectra of blends probably occurs because of the difference for creation of the singlet excitons [57]. When blends are excited by means of an absorption of photon in the case of photoluminescence, the excitons are created on PVK. The excitons are transferred to the guest P3 with a non-radiative manner. When the blends are excited by injection of electrons and holes, on the other hand, the charges are trapped on the P3 which has energy levels in the PVK. Therefore, neutral excitons are formed directly on the polymer. On the other hand, the solution PL spectra of the blends show very similar emission behavior with EL spectra. This means that the relaxations in EL occurs as if there is no aggregation between the chains and no quenching occurs. In other words PVK behaved as a matrix for the polymer besides transferring the charge carriers.

CHAPTER 4

CONCLUSION

Three novel D-A type alternating conjugated copolymers namely poly 4-(biphenyl-4-yl)-4'- tert butylspiro[benzo[d]imidazole-2,1'-cyclohexane] (P1), poly 4-(biphenyl-4-yl)-2-dodecyl-2H-benzo[d][1,2,3]triazole (P2) and poly(4-(5-(biphenyl-4-yl)-4-hexyl-thiophen-2-yl)-2-dodecyl-7-(4-hexylthiophen-2-yl)-2H-benzo[d][1,2,3]triazole (P3) were synthesized via Suzuki cross coupling polycondensation mechanism. Structural characteristics were confirmed by NMR analysis. Physical properties were investigated by GPC, TGA and DSC. Electrochemical characterizations were conducted by CV, spectroelectrochemistry and kinetic studies.

The polymers P2 and P3 have multicolored properties. On the contrary, the polymer P1 revealed violet color on its oxidized state and no color change was observed at its n-doped state. The convenient HOMO and LUMO values, thermal stabilities and strong absorption in the visible region indicates that the polymers have sufficient properties for thin film applications. Moreover kinetic studies of P2 and P3 reveal that they can be used for the ElectroChromic Device (ECD) applications.

Optical characterizations of the polymers reveal the relationship between the absorption and emission process. The bipenyl absorption is red-shifted by incorporating the BIm and BzT moieties and emission is tuned from blue to orange. The small stokes shift and spectral overlaps of absorption and emission, also desirable intensities of thin film emissions indicate that the polymers are applicable for OLED devices.

OLED device application of P3 with a device configuration of ITO/PEDOT:PSS/active layer/Ca/Al indicates that the results are quite desirable. Improvements for the outputs were done by blending PVK with various ratios of P3 for energy transfer studies.

The results indicate that energy transfer is accomplished for all the ratios but highest for 30 % acceptor ratio with optimum outputs.

Note that there were no other improvement studies such as solvent and thickness effect on the performance. The results could be further improved by various techniques. The three polymers have sufficient properties for OLED applications and by blending them with various ratios white light can be obtained. In addition to these both electrochromic and emission properties make the polymers good candidates for electrochromic light emitting devices.

REFERENCES

[1] C. K. Chiang, C. R. Fincher, Y. W. Park, A. J. Heeger, H. Shirakawa, E. J. Louis, S. C. Gau, and Alan G. MacDiarmid. Electrical conductivity in doped polyacetylene. *Phys. Rev. Lett.*, 39:1098–1101, Oct 1977.

[2] *Conducting Polymers (A New Era in Electrochemistry*. Berlin Heidelberg, 2008.

[3] Kai Zhang, Youtian Tao, Chuluo Yang, Han You, Yang Zou, Jingui Qin, and Dongge Ma. Synthesis and properties of carbazole main chain copolymers with oxadiazole pendant toward bipolar polymer host: Tuning the homo/lumo level and triplet energy. *Chemistry of Materials*, 20(23):7324–7331, 2008.

[4] Sachetan M. Tuladhar, Marc Sims, Stelios A. Choulis, Christian B. Nielsen, Wayne. N. George, Joachim H.G. Steinke, Donal D.C. Bradley, and Jenny Nelson. Influence of side chain symmetry on the performance of poly(2,5-dialkoxy-p-phenylenevinylene): fullerene blend solar cells. *Organic Electronics*, 10(4):562 – 567, 2009.

[5] *Principles of Polymerization*. John Wiley and Sons, 2004.

[6] *Modern Physical Organic Chemistry*. University Science Books, 2006.

[7] Frederik C Krebs. Electrochromic displays: The new black. *Nat Mater*, 2008.

[8] *Conducting Polymers, Fundamentals and Applications: A Practical Approach*. 1999.

[9] Avni A. Argun, Pierre-Henri Aubert, Barry C. Thompson, Irina Schwendeman, Carleton L. Gaupp, Jungseek Hwang, Nicholas J. Pinto, David B. Tanner, Alan G. MacDiarmid, and John R. Reynolds. Multicolored electrochromism in polymers: Structures and devices. *Chemistry of Materials*, 16(23):4401–4412, 2004.

[10] J. Roncali. Molecular engineering of the band gap of π-conjugated systems: Facing technological applications. *Macromolecular Rapid Communications*, 28(17):1761–1775, 2007.

[11] Xuejun Zhang and Samson A. Jenekhe. Electroluminescence of multicomponent conjugated polymers. 1. roles of polymer/polymer interfaces in emission enhancement and voltage-tunable multicolor emission in semiconducting polymer/polymer heterojunctions. *Macromolecules*, 33(6):2069–2082, 2000.

[12] Takakazu Yamamoto, Zhen-hua Zhou, Takaki Kanbara, Masaki Shimura, Kenichi Kizu, Tsukasa Maruyama, Yoshiyuki Nakamura, Takashi Fukuda, Bang-Lin Lee, Naoki Ooba, Satoru Tomaru, Takashi Kurihara, Toshikuni Kaino, Kenji Kubota, and Shintaro Sasaki. π-conjugated donor-acceptor copolymers

constituted of π-excessive and π-deficient arylene units. optical and electrochemical properties in relation to ct structure of the polymer. *Journal of the American Chemical Society*, 118(43):10389–10399, 1996.

[13] Abasaheb V. Patil, Woo-Hyung Lee, Eunwoo Lee, Kyuri Kim, In-Nam Kang, and Soo-Hyoung Lee. Synthesis and photovoltaic properties of a low-band-gap copolymer of dithieno[3,2-b:2',3'-d]thiophene and dithienylquinoxaline. *Macromolecules*, 44(6):1238–1241, 2011.

[14] E.R. Kötz, H. Neff, and K. Müller. A ups, xps and work function study of emersed silver, platinum and gold electrodes. *Journal of Electroanalytical Chemistry and Interfacial Electrochemistry*, 215:331 – 344, 1986.

[15] Pierre M. Beaujuge and John R. Reynolds. Color control in /*pi*-conjugated organic polymers for use in electrochromic devices. *Chemical Reviews*, 110(1):268–320, 2010. PMID: 20070115.

[16] Lemmer U., Heun S., Mahrt R.F., Scherf U., Hopmeier M., Siegner U., Gobel E.O., Mullen K., and Bassler H. Aggregate fluorescence in conjugated polymers. *Chemical Physics Letters*, 240(4):373–378, 1995.

[17] J. W. Blatchford, S. W. Jessen, L.-B. Lin, T. L. Gustafson, D.-K. Fu, H.-L. Wang, T. M. Swager, A. G. MacDiarmid, and A. J. Epstein. Photoluminescence in pyridine-based polymers: Role of aggregates. *Phys. Rev. B*, 54:9180–9189, Oct 1996.

[18] Gerwin H. Gelinck, Emiel G.J. Staring, Do-Hoon Hwang, George C.W. Spencer, Andrew B. Holmes, and John M. Warman. The effect of broken conjugation and aggregation on photo-induced charge separation on polyphenylenevinylene chains. *Synthetic Metals*, 84:595 – 596, 1997. International Conference on Science and Technology of Synthetic Metals.

[19] J. Kalinowski. Excimers and exciplexes in organic electroluminescence. *Materials Science-Poland*, 2009.

[20] Thuc-Quyen Nguyen, Raymond C. Kwong, Mark E. Thompson, and Benjamin J. Schwartz. Higher efficiency conjugated polymer-based leds by control of polymer film morphology and interchain interactions. *Synthetic Metals*, 119:523 – 524, 2001. Proceedings of the International Conference on Science and technology of Synthetic Metals.

[21] Christopher J. Collison, Lewis J. Rothberg, Varaporn Treemaneekarn, and Yi Li. Conformational effects on the photophysics of conjugated polymers: A two species model for meh-ppv spectroscopy and dynamics. *Macromolecules*, 34(7):2346–2352, 2001.

[22] Paul F. Barbara, Andre J. Gesquiere, So-Jung Park, and Young Jong Lee. Single-molecule spectroscopy of conjugated polymers. *Accounts of Chemical Research*, 38(7):602–610, 2005.

[23] Thomas Huser, Ming Yan, and Lewis J. Rothberg. Single chain spectroscopy of conformational dependence of conjugated polymer photophysics. *Proceedings of the National Academy of Sciences*, 97(21):11187–11191, 2000.

[24] Benjamin J. Schwartz. Conjugated polymers as molecular materials: How chain conformation and film morphology influence energy transfer and interchain interactions. *Annual Review of Physical Chemistry*, 54(1):141–172, 2003.

[25] *Modern Molecular Photochemistry*. University Science Books, 1991.

[26] *Fluorescence and Phosphorescence Spectroscopy: Physicochemical Principles and Practiec*. Pergamon Press, 1977.

[27] *Fundamentals of Organic Chemistry*. John Wiley and Sons, 1978.

[28] Th. Förster. Zwischenmolekulare energiewanderung und fluoreszenz. *Annalen der Physik*, 437(1-2):55–75, 1948.

[29] D. L. Dexter. A theory of sensitized luminescence in solids. *The Journal of Chemical Physics*, 21(5):836–850, 1953.

[30] *Electronic Processes in Organic Crystals and Polymers*. Oxford University Press, 1999.

[31] W. Helfrich and W. G. Schneider. Recombination radiation in anthracene crystals. *Phys. Rev. Lett.*, 14:229–231, Feb 1965.

[32] C. W. Tang, S. A. VanSlyke, and C. H. Chen. Electroluminescence of doped organic thin films. *Journal of Applied Physics*, 65(9):3610–3616, 1989.

[33] Chihaya Adachi, Tetsuo Tsutsui, and Shogo Saito. Organic electroluminescent device having a hole conductor as an emitting layer. *Applied Physics Letters*, 55(15):1489–1491, 1989.

[34] J. H. Burroughes, D. D. C. Bradley, A. R. Brown, R. N. Marks, K. Mackay, R. H. Friend, P. L. Burns, and A. B. Holmes. Light-emitting diodes based on conjugated polymers. *Nature*, 1990.

[35] James R. Sheats, Homer Antoniadis, Mark Hueschen, William Leonard, Jeff Miller, Ron Moon, Daniel Roitman, and Andrew Stocking. Organic electroluminescent devices. *Science*, 273(5277):884–888, 1996.

[36] M. Hack. Oleds: The history and future trends. presentation.

[37] P. Anderson. Polymer oled displays. Technical report, Philips Research Public Relations Dept, 2004.

[38] http://www.oled-info.com/micromax-pixel-a90-photo, [last accessed: 30/08/2012].

[39] Motoshi Shibata, Yoshiki Nitta, Ken Fujita, and Masakazu Ichikawa. Pyramidal si nanocrystals with a quasiequilibrium shape selectively grown on si(001) windows in ultrathin sio_2 films. *Phys. Rev. B*, 61:7499–7504, Mar 2000.

[40] Y Cao, G Yu, C Zhang, R Menon, and A.J Heeger. Polymer light-emitting diodes with polyethylene dioxythiophene-polystyrene sulfonate as the transparent anode. *Synthetic Metals*, 87(2):171 – 174, 1997.

[41] M. A. Baldo and S. R. Forrest. Interface-limited injection in amorphous organic semiconductors. *Phys. Rev. B*, 64:085201, Aug 2001.

[42] Antoine Kahn, Norbert Koch, and Weiying Gao. Electronic structure and electrical properties of interfaces between metals and π-conjugated molecular films. *Journal of Polymer Science Part B: Polymer Physics*, 41(21):2529–2548, 2003.

[43] H Murata, G.G Malliaras, M Uchida, Y Shen, and Z.H Kafafi. Non-dispersive and air-stable electron transport in an amorphous organic semiconductor. *Chemical Physics Letters*, 339:161 – 166, 2001.

[44] Mukundan Thelakkat. Star-shaped, dendrimeric and polymeric triarylamines as photoconductors and hole transport materials for electro-optical applications. *Macromolecular Materials and Engineering*, 287(7):442–461, 2002.

[45] R. A. Marcus. On the theory of oxidation-reduction reactions involving electron transfer. i. *The Journal of Chemical Physics*, 24(5):966–978, 1956.

[46] A.R. Brown, K. Pichler, N.C. Greenham, D.D.C. Bradley, R.H. Friend, and A.B. Holmes. Optical spectroscopy of triplet excitons and charged excitations in poly(p-phenylenevinylene) light-emitting diodes. *Chemical Physics Letters*, 210:61 – 66, 1993.

[47] M. A. Baldo, D. F. O'Brien, M. E. Thompson, and S. R. Forrest. Excitonic singlet-triplet ratio in a semiconducting organic thin film. *Phys. Rev. B*, 60:14422–14428, Nov 1999.

[48] Abidin Balan, Derya Baran, Gorkem Gunbas, Asuman Durmus, Funda Ozyurt, and Levent Toppare. One polymer for all: benzotriazole containing donor-acceptor type polymer as a multi-purpose material. *Chem. Commun.*, pages 6768–6770, 2009.

[49] Ya-Hsien Tseng, Ping-I Shih, Chen-Han Chien, Ajay Kumar Dixit, Ching-Fong Shu, Yi-Hung Liu, and Gene-Hsiang Lee. Stable organic blue-light-emitting devices prepared from poly[spiro(fluorene-9,9'-xanthene)]. *Macromolecules*, 38(24):10055–10060, 2005.

[50] Fluorescence standard reference material: quinine sulfate dihydrate. *Appl. Opt.*, 20(9):1718, May 1981.

[51] Xi Chen, He Wan, Haidong Li, Fengmei Cheng, Wei Nie, Bing Yao, Zhiyuan Xie, Lixiang Wang, and Jidong Zhang. The influence of residue aggregation in solution on photoluminescence and electroluminescence of polyoctylfluorene thin film. *Organic Electronics*, 13(3):475 – 482, 2012.

[52] P Schouwink, A.H Sch afer, C Seidel, and H Fuchs. The influence of molecular aggregation on the device properties of organic light emitting diodes. *Thin Solid Films*, 372:163 – 168, 2000.

[53] Jeong-Ik Lee, Genit Klaemer, and Robert D. Miller. Structure-property relationship for excimer formation in poly(alkylfluorene) derivatives. *Synthetic Metals*, 101:126 –, 1999. International Conference on Science and Technology of Synthetic.

[54] Yong Qiu, Lian Duan, Xiaoming Hu, Deqiang Zhang, Min Zheng, and Fenglian Bai. Electroluminescence enhancement by blending pvk with an alternating

copolymer containing triphenylamine and phenylene units. *Synthetic Metals*, 123(1):39 – 42, 2001.

[55] C. Gabriel, B. nd Ana and M. Jorge. Luminescence properties of poly(9,9-dioctylfluorene)/polyvinylcarbazole blends: Role of composition on the emission colour stability and electroluminescence efficiency. *Journal of Physics and Chemistry of Solids*, 2010.

[56] K. B. Eisenthal and S. Siegel. Influence of resonance transfer on luminescence decay. *The Journal of Chemical Physics*, 41(3):652–655, 1964.

[57] M. D. McGehee, T. Bergstedt, C. Zhang, A. P. Saab, M. B. O'Regan, G. C. Bazan, V. I. Srdanov, and A. J. Heeger. Narrow bandwidth luminescence from blends with energy transfer from semiconducting conjugated polymers to europium complexes. *Advanced Materials*, 11(16):1349–1354, 1999.

Appendix A

APPENDIX A

A.1 TGA OF P1

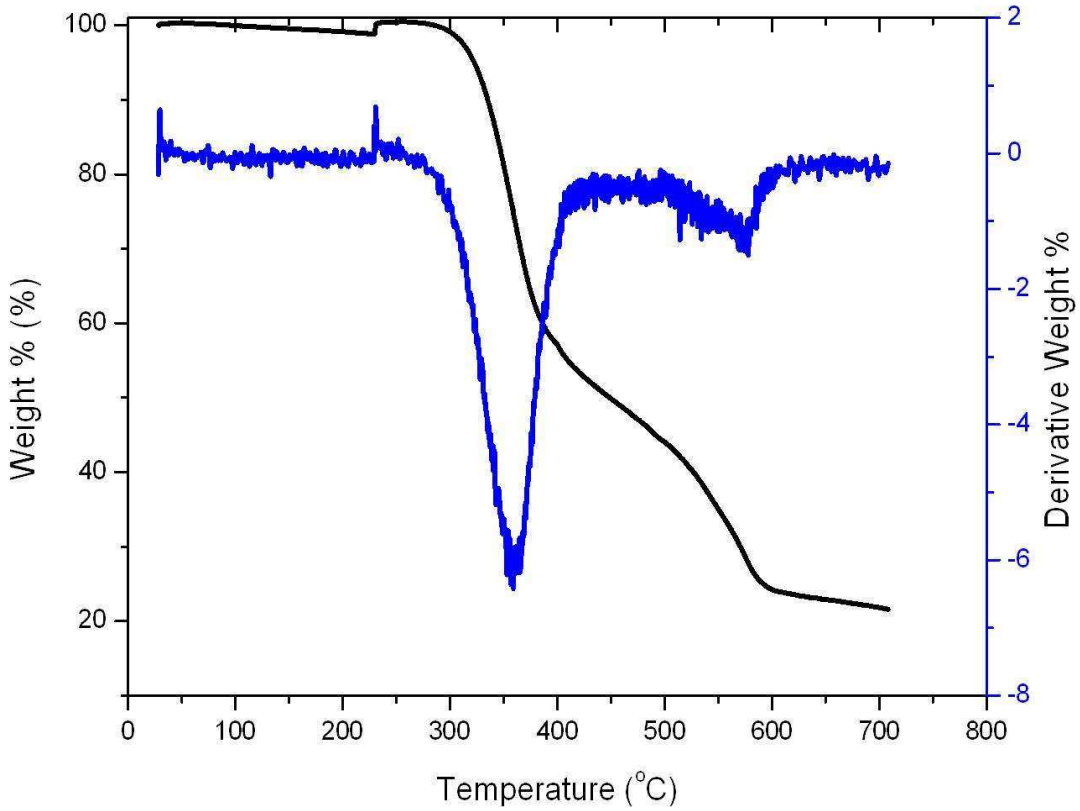

Figure A.1: TGA result of P1

A.2 TGA OF P2

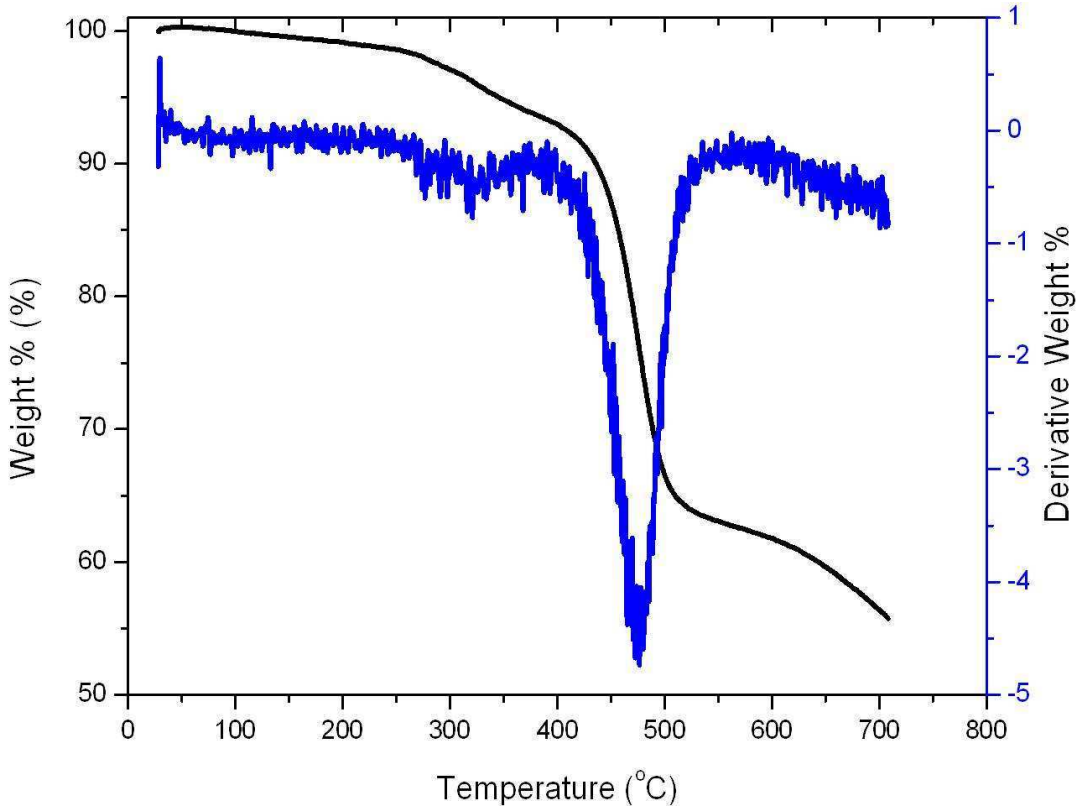

Figure A.2: TGA result of P2

A.3 TGA OF P3

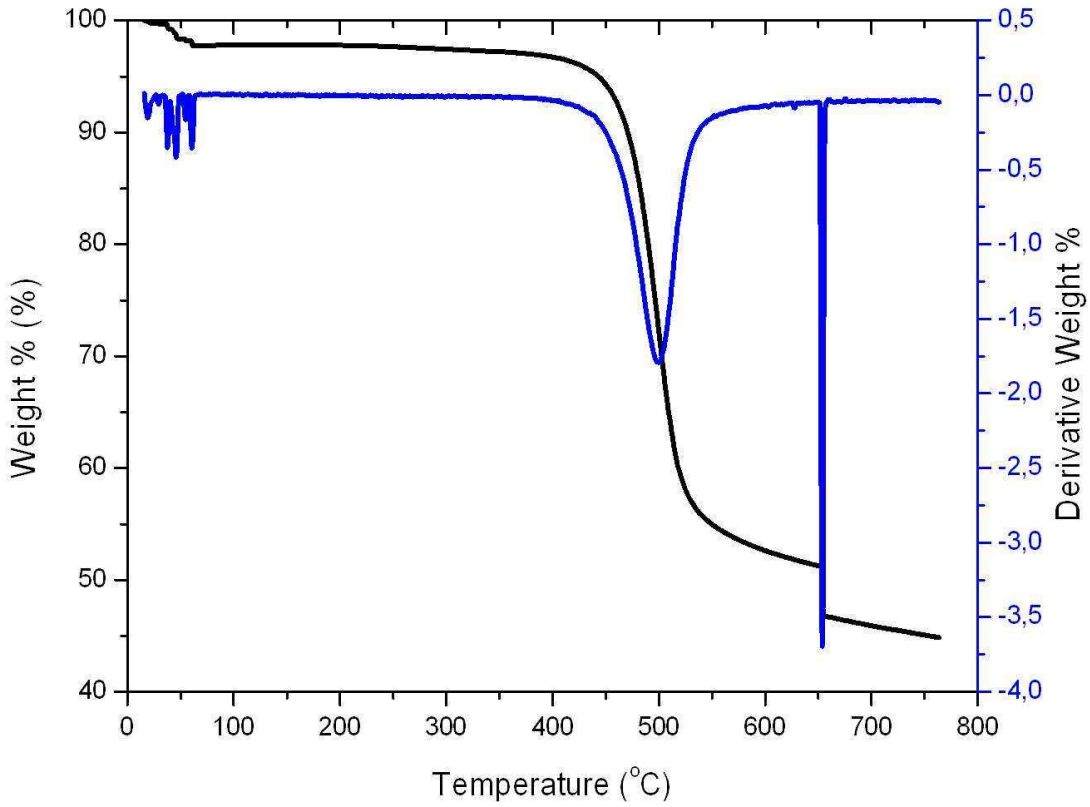

Figure A.3: TGA result of P3

Appendix B

APPENDIX B

B.1 DSC OF P1

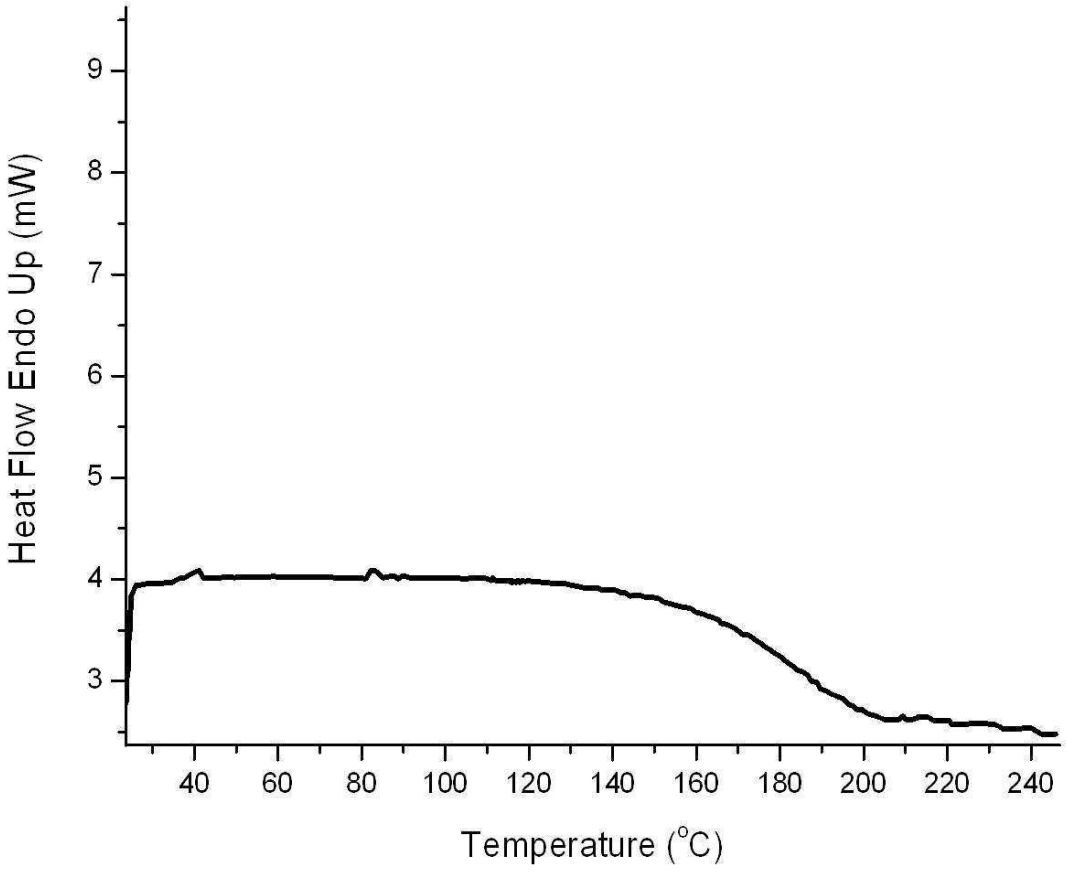

Figure B.1: DSC result of P1

B.2 DSC OF P2

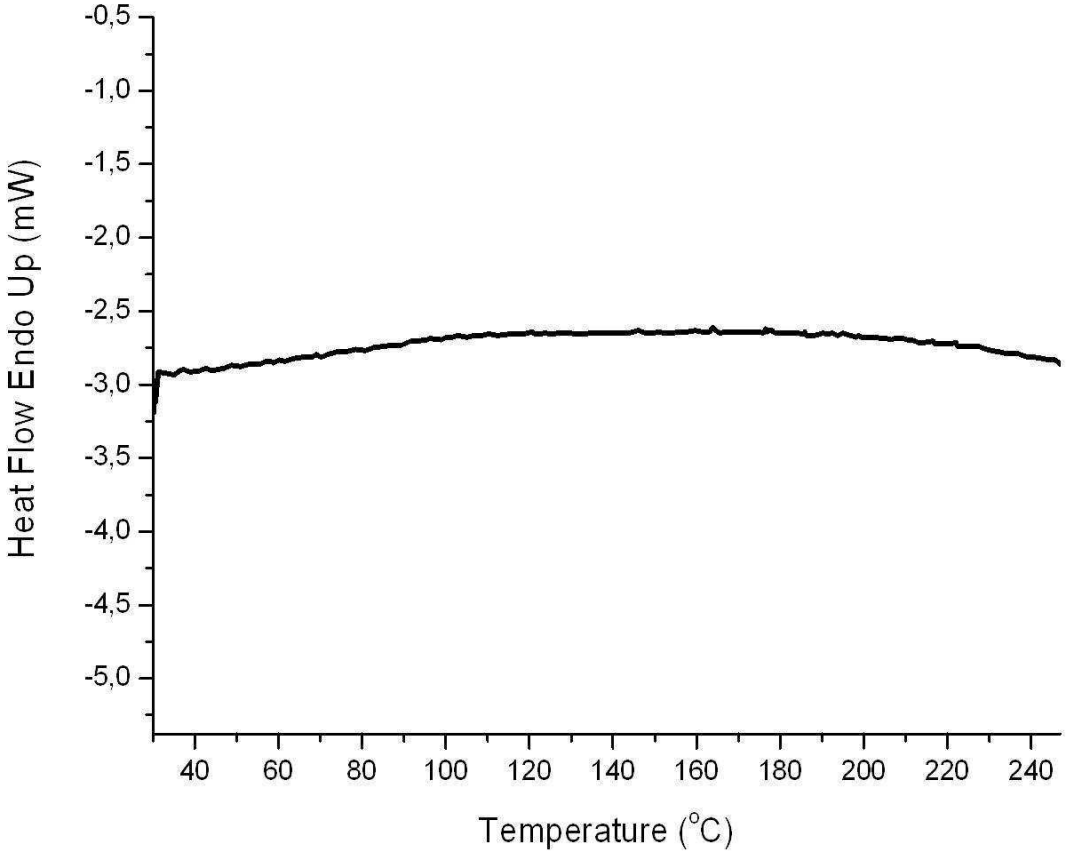

Figure B.2: DSC result of P2

B.3 DSC OF P3

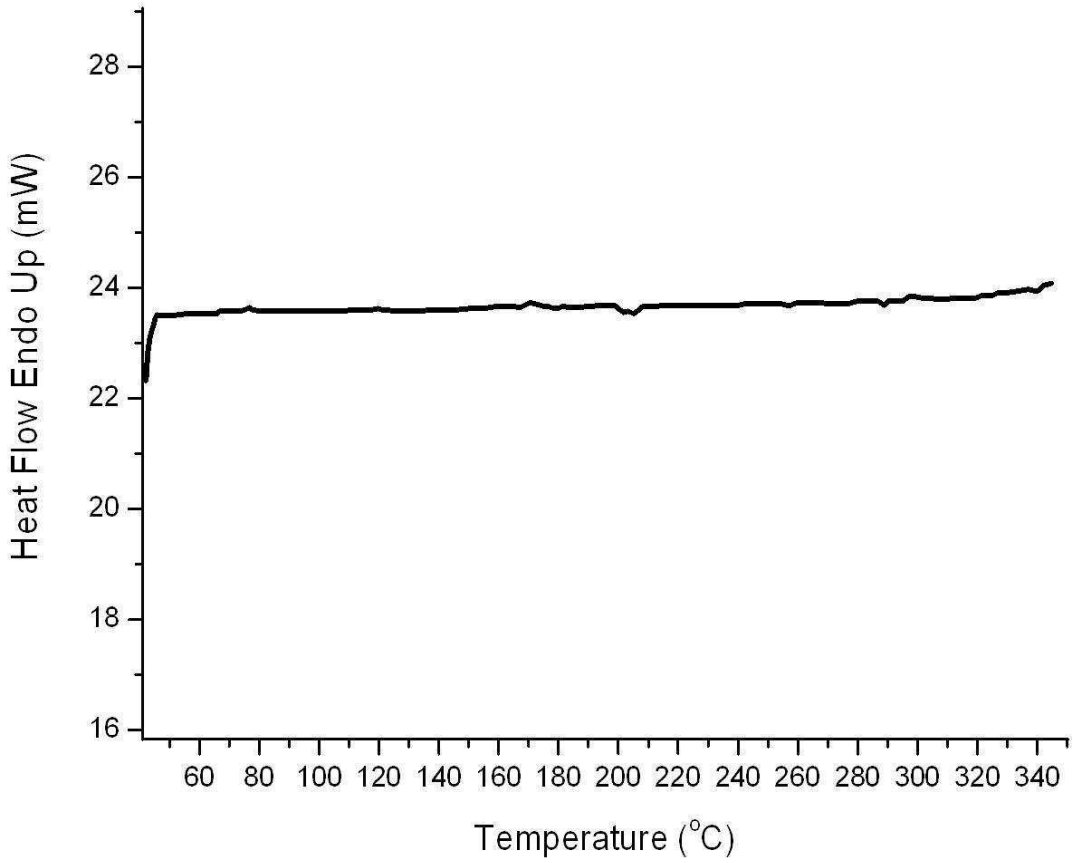

Figure B.3: DSC result of P3